2020-03

SMALL-SCALE ENERGY EXTRACTION FOR COMPRESSED AIR ENERGY STORAGE USING POSITIVE DISPLACEMENT RADIAL AIR MOTOR

Johnson, Michael S.

Monterey, CA; Naval Postgraduate School

NAVAL POSTGRADUATE SCHOOL

MONTEREY, CALIFORNIA

THESIS

SMALL-SCALE ENERGY EXTRACTION FOR COMPRESSED AIR ENERGY STORAGE USING POSITIVE DISPLACEMENT RADIAL AIR MOTOR

by

Michael S. Johnson

March 2020

Thesis Advisor: Anthony J. Gannon
Co-Advisor: Walter Smith

THIS PAGE INTENTIONALLY LEFT BLANK

REPORT DOCUMENTATION PAGE	*Form Approved OMB No. 0704-0188*

1. AGENCY USE ONLY *(Leave blank)*	**2. REPORT DATE** March 2020	**3. REPORT TYPE AND DATES COVERED** Master's thesis

4. TITLE AND SUBTITLE SMALL-SCALE ENERGY EXTRACTION FOR COMPRESSED AIR ENERGY STORAGE USING POSITIVE DISPLACEMENT RADIAL AIR MOTOR	**5. FUNDING NUMBERS**
6. AUTHOR(S) Michael S. Johnson	
7. PERFORMING ORGANIZATION NAME(S) AND ADDRESS(ES) Naval Postgraduate School Monterey, CA 93943-5000	**8. PERFORMING ORGANIZATION REPORT NUMBER**
9. SPONSORING / MONITORING AGENCY NAME(S) AND ADDRESS(ES) N/A	**10. SPONSORING / MONITORING AGENCY REPORT NUMBER**

11. SUPPLEMENTARY NOTES The views expressed in this thesis are those of the author and do not reflect the official policy or position of the Department of Defense or the U.S. Government.

12a. DISTRIBUTION / AVAILABILITY STATEMENT Approved for public release. Distribution is unlimited.	**12b. DISTRIBUTION CODE** A

13. ABSTRACT (maximum 200 words)

Compressed Air Energy Storage (CAES) provides a unique and environmentally friendly solution to problems posed with other renewable energy systems. Solar and wind have peak generation times that do not correspond to peak usage times. Using CAES allows for the storage of that excess energy to be used later or to charge battery/capacitor banks when solar and wind are not available. Manufacture and maintenance of compressed air (CA) systems is inexpensive and CA infrastructure already exists through pneumatic tool and control systems. CAES systems range in size from the large scale (hundreds of megawatts) to the microscale (3 kilowatts). Micro to small-scale applications are ideal for existing system or microgrid integration and field mobility. Various methods of prime movers may be used in CAES generation plants, including turbines and different types of positive displacement motors. Small and microscale units will work with turbines but have difficulty with using large volumes of air with low torque generation. This thesis explored the use of a positive displacement air motor as the prime mover with a commercially available 3-phase motor repurposed as a generator to charge a super-capacitor, while all were fitted inside of a small, easily transportable container.

14. SUBJECT TERMS Compress Air Energy Storage, CAES, air motor, capacitor, super-capacitor, energy extraction, energy storage, generator	**15. NUMBER OF PAGES** 93
	16. PRICE CODE

17. SECURITY CLASSIFICATION OF REPORT	**18. SECURITY CLASSIFICATION OF THIS PAGE**	**19. SECURITY CLASSIFICATION OF ABSTRACT**	**20. LIMITATION OF ABSTRACT**
Unclassified	Unclassified	Unclassified	UU

NSN 7540-01-280-5500 Standard Form 298 (Rev. 2-89) Prescribed by ANSI Std. 239-18

THIS PAGE INTENTIONALLY LEFT BLANK

Approved for public release. Distribution is unlimited.

SMALL-SCALE ENERGY EXTRACTION FOR COMPRESSED AIR ENERGY STORAGE USING POSITIVE DISPLACEMENT RADIAL AIR MOTOR

Michael S. Johnson
Lieutenant, United States Navy
BSAST, Thomas A Edison State College, 2012

Submitted in partial fulfillment of the
requirements for the degree of

MASTER OF SCIENCE IN MECHANICAL ENGINEERING

from the

NAVAL POSTGRADUATE SCHOOL
March 2020

Approved by: Anthony J. Gannon
Advisor

Walter Smith
Co-Advisor

Garth V. Hobson
Chair, Department of Mechanical and Aerospace Engineering

THIS PAGE INTENTIONALLY LEFT BLANK

ABSTRACT

Compressed Air Energy Storage (CAES) provides a unique and environmentally friendly solution to problems posed with other renewable energy systems. Solar and wind have peak generation times that do not correspond to peak usage times. Using CAES allows for the storage of that excess energy to be used later or to charge battery/capacitor banks when solar and wind are not available. Manufacture and maintenance of compressed air (CA) systems is inexpensive and CA infrastructure already exists through pneumatic tool and control systems. CAES systems range in size from the large scale (hundreds of megawatts) to the microscale (3 kilowatts). Micro to small-scale applications are ideal for existing system or microgrid integration and field mobility. Various methods of prime movers may be used in CAES generation plants, including turbines and different types of positive displacement motors. Small and microscale units will work with turbines but have difficulty with using large volumes of air with low torque generation. This thesis explored the use of a positive displacement air motor as the prime mover with a commercially available 3-phase motor repurposed as a generator to charge a super-capacitor, while all were fitted inside of a small, easily transportable container.

THIS PAGE INTENTIONALLY LEFT BLANK

TABLE OF CONTENTS

LIST OF FIGURES

LIST OF TABLES

THIS PAGE INTENTIONALLY LEFT BLANK

LIST OF ACRONYMS AND ABBREVIATIONS

AC	alternating current
CAES	Compressed Air Energy Storage
CA	compressed air
DAQ	data acquisition
DOD	Department of Defense
DC	direct current
HP	horsepower
I/O	input/output
kPa	kilopascals
KV	RPM per Volt
kW	kilowatt
MW	Megawatt
NI	National Instruments
PLA	Polylactic Acid
PSIG	pounds per square inch gauge
RPM	revolutions per minute
SCFM	standard cubic feet per minute
SS	stainless steel
W	Watt(s)
V	Volt(s)

THIS PAGE INTENTIONALLY LEFT BLANK

EXECUTIVE SUMMARY

The Department of the Navy (DoN) and the Department of Defense (DOD) began an initiative in 2016 to strengthen the energy resilience of the DoN with the idea to decrease the dependence of the DOD/DoN on the surrounding electrical grids and to develop and install microgrids on installations. The Resilient Energy Program Office (REPO) "executes energy resilience, alternative energy and renewable energy projects with the mission to enhance the DON"s energy resilience" [1]. In keeping with this emphasis on resilient energy, compressed air energy storage, and the subsequent extraction, use existing technologies, equipment, and infrastructures in a manner not normally seen.

Using a commercially available air motor to drive a quad-copter motor as a generator, electricity can be generated and converted to direct current (DC) to run equipment, charge batteries, or in this case, charge super-capacitors. This research brings inexpensive items together to bring a super-capacitor from completely discharged to full 56 Volts in less than 700 seconds (11.3 minutes). Using additive manufacturing, technical problems that arose were easily dealt with, bringing repairability of the unit within the capabilities of the end user. The entire apparatus fits together inside of a self-contained unit for easy transport and installation to any compressed air source. The use of a positive displacement air motor increases efficiency at the small-scale [2], allowing for the best use of the available air supply versus a large turbine as seen on the industrial/utility scale.

This system could be further optimized to further reduce air consumption and made smaller to allow for man-portable systems. At the best performance, the system uses 8.65 cubic meters of air, approximately the same volume of in three standard SCUBA tanks at 20 MPa (3000 PSI) to fully charge a 56V/130F super-capacitor from discharged to fully charged. Responsible use of the system, using it only to maintain the voltage above a certain level would use even less air, creating a system that could maintain voltage of a battery or capacitor bank on a relatively small volume of air.

Compressed air, when compared to that of Li-ion batteries, does not have an impressive energy density and can be easily discounted as a storage medium [3]. However

compressed air performance is not dependent on a small temperature range for operation nor the hazards associated with Li-ion. Further, compressed air has an infinite number of cycles, whereas batteries decrease in performance over time. Robust compressed air infrastructure already exists throughout the DoN at the shore installations and aboard ships. Air compressors come in many sizes, able to compress air from low pressure to high pressure. Integration with existing systems is simply a "plug and play" connection with standardized air fittings. This system can operate on air pressures as low as 206 kPa (30 PSI), allowing any compressed air source to be reduced down to drive the air motor. Versatility, utility, resiliency, and portability describe the small-scale CAES extraction system.

References

[1] US Navy Energy, Environment and Climate Change "Resilient Energy Program Office," accessed February 26, 2020, https://navysustainability.dodlive.mil/energy/repo-3/References

[2] He, W. and Wang, J, 2018, "Optimal selection of air expansion machine in Compressed Air Energy Storage: A Review," *Renewable and Sustainable Energy Reviews, 87*, pp 77–95.

[3] Luo, X., Wang, J., Dooner, M., Clarke, J., 2014, "Overview of current development in electrical energy storage technologies and the application potential in power system operation," *Applied Energy* 137, pp. 511–536

ACKNOWLEDGMENTS

I’d like to thank my wife and children for their patience over the last couple of years. Thank you to my thesis advisors, Dr. Gannon and Dr. Smith, for your assistance and patience throughout the process as well.

Heavy thanks to Dan and Danny for helping me get up to speed for my first foray into a classroom setting since high school. You guys helped keep me relaxed and focused.

To my parents… I wish you could have been here and I hope I’ve made you proud. I miss you.

THIS PAGE INTENTIONALLY LEFT BLANK

I. LITERATURE REVIEW

A. COMPRESSED AIR ENERGY STORAGE—CURRENT STATE OF THE ART

There are currently several large-scale Compressed Air Energy Storage (CAES) systems in place in the world. Ramadan et al., examined two that have existed for several decades, located in Germany and Alabama, in their article for the International Journal of Low-Carbon Technologies [1]. These plants use compressed air as part of a Brayton Cycle power generation system. They conducted an analysis on the use of CAES regarding the Suez Region of Egypt, integrating with the existing wind farms in the area. From the large scale to the micro and small-scale, CAES has the potential to be very versatile in its available uses. CAES Systems on the large scale use turbines to extract the energy while small and micro-scale systems are built using positive displacement motors as the prime mover. Regardless of the scale, the concept is the same: a device is used to expand the compressed air, converting the stored energy into electricity through the rotary motion of a generator. Large-scale applicability requires significant investment in material and real estate, often with areas encompassing natural caves or other similar geologic formations to store the compressed air. There are ways to store the compressed air underwater, using the hydrostatic force of the water column to provide constant pressure air, but this also requires a large area with potential hazards to the air reserve from vessels or unseen bottom objects. Furthermore, to get one atmosphere of air pressure, there needs to be a ten meter of water column above the air reservoir. Higher atmospheres of pressure would require water depths in the hundreds of meters to have viable air pressure. Small-scale systems are more applicable to microgrid integration and require substantially less of a monetary investment to install and maintain, as discussed by He and Wang in their Renewable and Sustainable Energy Reviews article [2]. Air flasks of various sizes are inexpensive and when compared with the sizing of batteries or capacitors of the same cost and energy density, are potentially much smaller [2]. Figure 1 and Figure 2 show different options for storing compressed air, such as salt caves and underwater bladders. Table 1 shows the comparisons between various energy storage mediums and systems.

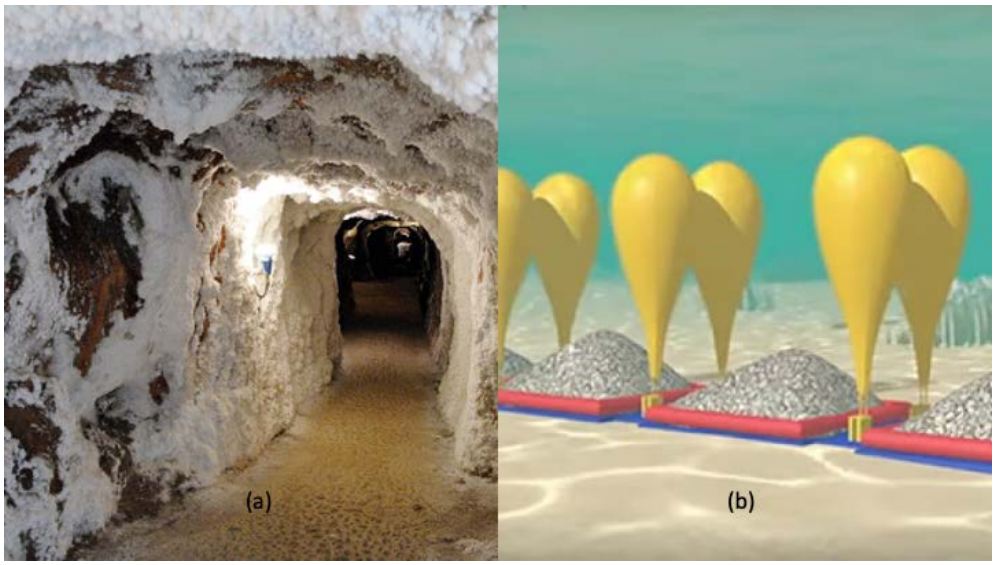

(a) Adapted from https://theconversation.com/lets-store-solar-and-wind-energy-by-using-compressed-air-103183; (b) adapted from [10].

Figure 1. Compressed Air Storage Options: Salt Mines/Caverns Used for Large-Scale CAES

Figure 2. Air Flasks Used for General Purpose Compressed Air Storage. Adapted from [11].

Table 1. Characteristics of Various Energy Storage Systems. Source: [2].

Characteristics	Large-scale CAES	Small CAES	PHES	Li-ion battery	Lead acid battery	Super-capacity	Hydrogen fuel
Power density, W/L	0.5–2	> large-scale CAES	0.5–1.5	1500–10,000	10–400	> 100,000	> 500
Energy density, Wh/L	2–6	> large-scale CAES	0.5–2	200–500	50–90	10–30	500–3000
Rated power rating, MW	100–1000	0.003–3 potential to 10	100–5000	0–100	0–40	0–0.3 +	< 50
Rated energy capacity, MWh	< 1000	< ~ 0.01	500–8000	0–10	0–40	0–0.0005	0.312 and 39
Lifetime, year	20–40	> 23	40–60	5–16	5–15	10–30	5–20
Cycle efficiency	40–70%	–	70–85%	75–97%	63–90%	84–95%	20–66%
Response time	Minutes	Seconds-minutes	Minutes	Milli-seconds	Milli-seconds	Milli-seconds	Seconds
Power capital cost, $/kWh	400–1000	517–1550	2000–4000	900–4000	300–600	100–450	500–3000
Energy capital cost, $/kWh	2–120	200–250	5–100	600–3800	200–400	300–2000	2–15

Earlier research, conducted by McLaughlin [3] and Pelletier [4], used an automotive turbocharger as a turbine prime mover and then with an air ejector added to increase the mass flow rate of the air through the turbine. Both systems were found to lack the required torque to adequately charge the attached super-capacitor during heavy load conditions, in keeping with the research completed by He and Wang [2]. Further, their systems used large amounts of compressed air.

B. CAES SHORESIDE APPLICABILITY

The use of CAES at naval installations is a plausible transition due to the abundance of compressed air systems already in place, especially at maintenance facilities using pneumatic tool systems. Installed microgrids, made up of solar and wind generators combined with air compressors to store excess during low demand periods or when grid power is at its lowest cost, allows buildings containing sensitive electronic equipment to have continuity of power, thus increasing resilience. Solar and wind energy are easily harnessed but are subject to the whims of the environment and weather. Uncharacteristically cloudy days or seasonal weather patterns that reduce the amount of available wind and sun greatly impact the power generation. Compounding the problem are the peak “usage” times versus the peak “generation” times, often with the two not lined up. Storage of excess energy during the peak generation periods is essential to offsetting the demand during the peak usage times. Batteries have been the historically relied upon storage option for that excess due to simplicity and minimal expense. Continuity of power is a necessity for shore installations, regardless of their purpose. Loss of power to a facility that provides services to the fleet (i.e., communication hubs, water space

management and deconfliction, in-port services) could have disastrous effects if the service is not immediately restored. CAES provides an alternative (or an additional option) for use in storing excess energy.

C. SMALL-SCALE CAES SYSTEMS

Small-scale systems are typically less than 10 kW in available power, for use in microgrid applications. Their size allows for mobility and adaptability into existing systems. With the smaller scale, inefficient use of the air reserve has a much larger impact than on the large scale due to the small air reserve. He and Wang's research has shown that small and microscale systems have a higher cycle efficiency when using positive displacement prime movers rather than the turbine types, typically seen in the large industrial scale systems [2]. Small-scale systems allow for versatility and mobility with the unit due to the inherent compact nature and small components. This permits bolt on usability and quick deployment of a ready-made, self-contained portable system. McLaughlin's proof of concept with a turbocharger as the motive force showed that compressed air could indeed be used to adequately charge supercapacitors [3]. Pelletier's work with a turbocharger and air ejector aimed to improve that efficiency by entraining additional mass from the surrounding atmosphere into the turbocharger. This overcame the difficulties seen when the system was under increased load. While this was effective in increasing performance, overall air consumption was too high to make the system viable [4].

1. Turbocharger Powered

Proof of concept was completed by McLaughlin with his research on a small-scale air driven generator [3]. His work highlighted the proof of concept of the system, showing that a system comprised of small components could charge a supercapacitor. Limitations associated with using a turbine as the prime mover with the small-scale system are associated with the higher torque required at towards the end of the charging cycle when the current flow is lowest from the increased impedance of the capacitor. His work was able to charge a 16V/500 F super-capacitor to approximately 11 Volts in 2500 seconds (~41.7 minutes). His posited that if additional mass flow were entrained into the working fluid prior to entering the turbine, efficiency would be increased, which was further explored in Pelletier's follow on work [3,4].

2. Turbocharger with Air Ejector

Pelletier, building on the McLaughlin's previous work, added an air ejector into the system to increase the mass flow rate into the system [4]. Both systems were able to charge the 16 V/500 F super-capacitor, with Pelletier's work expanding and charging a 56 V/130 F super-capacitor in approximately six minutes at 0.05 m^3/s (102 SCFM). Turbines use large amounts of air mass to convert the energy into rotary motion. Work done by He and Wang showed that to increase cycle efficiency, positive displacement motors are better suited for small-scale operations instead of turbines [2].

D. SYSTEM SCHEMATIC USED IN THIS STUDY

The system described was built with commercially available, off the shelf items and assembled into a self-contained unit for transport and use. Component descriptions and performance characteristics will be discussed further in Chapter II. Figure 3 shows the line diagram schematic of the completed small-scale extraction system. The completed system has a ten times voltage step up from the voltage produced by the 3-phase generator with individual phase transformers. Figure 4 is a photo of the completed system.

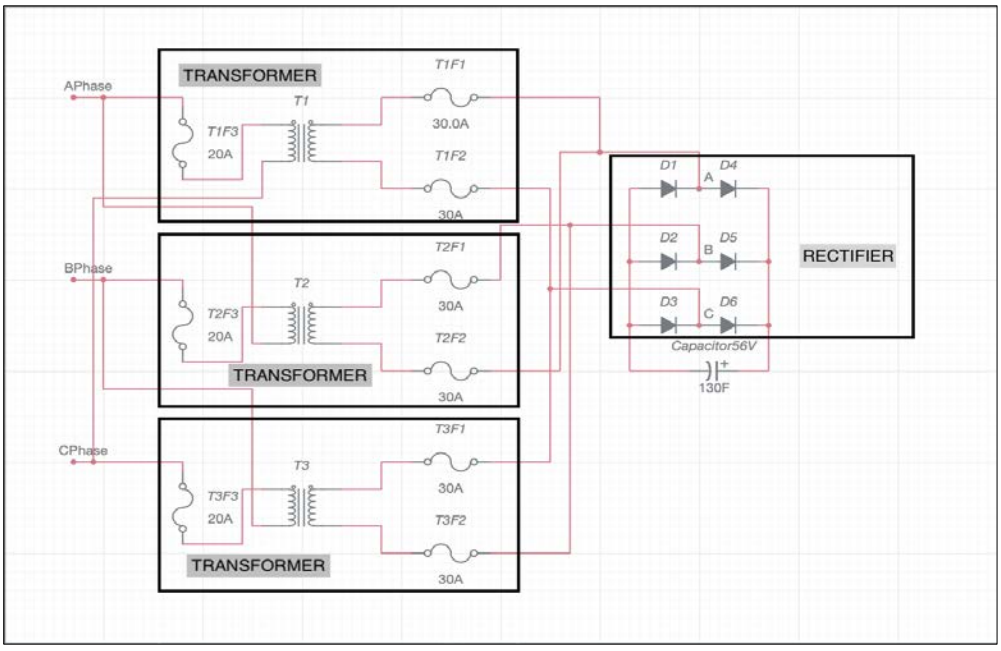

Figure 3. Line Diagram Schematic of Completed Project (Not to Scale)

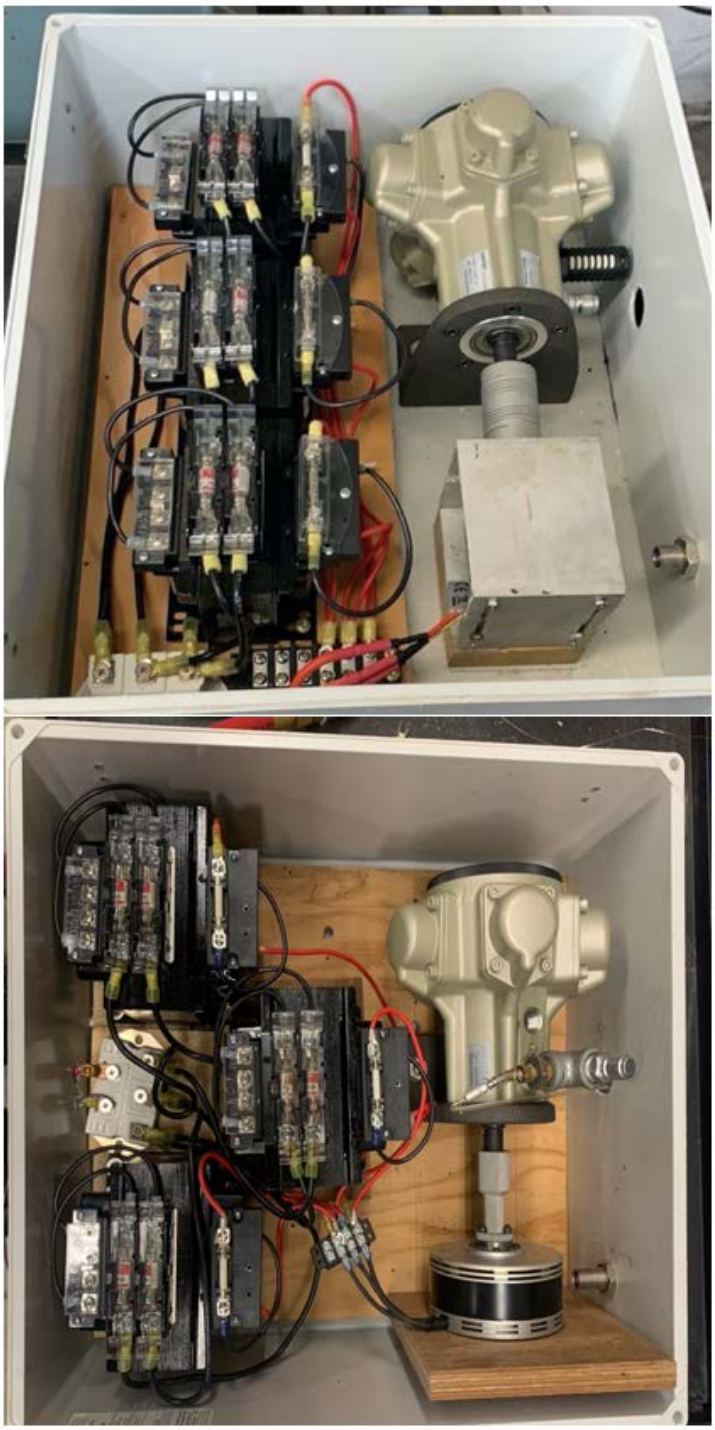

Figure 4. Completed System, Shown with 150 KV PMG (top) and 80 KV PMG (bottom)

II. COMPONENT TECHNICAL DATA

A. AIR MOTOR

Previous research had used automotive turbos as the prime mover had been ineffective at efficiently producing usable power from CAES reserves [3,4]. He and Wang's research showed that for micro and small-scale applications of CAES, a positive displacement motor increases the cycle efficiency, allowing for more charge cycles from the same volume of air [2]. The air motor used in this arrangement is a five cylinder, .31 HP radial air motor, specifically the UTAM4-030 model (Figure 6), from AirOil, Inc. Optimal expander selection based upon desired specific speed can be seen in Figure 5.

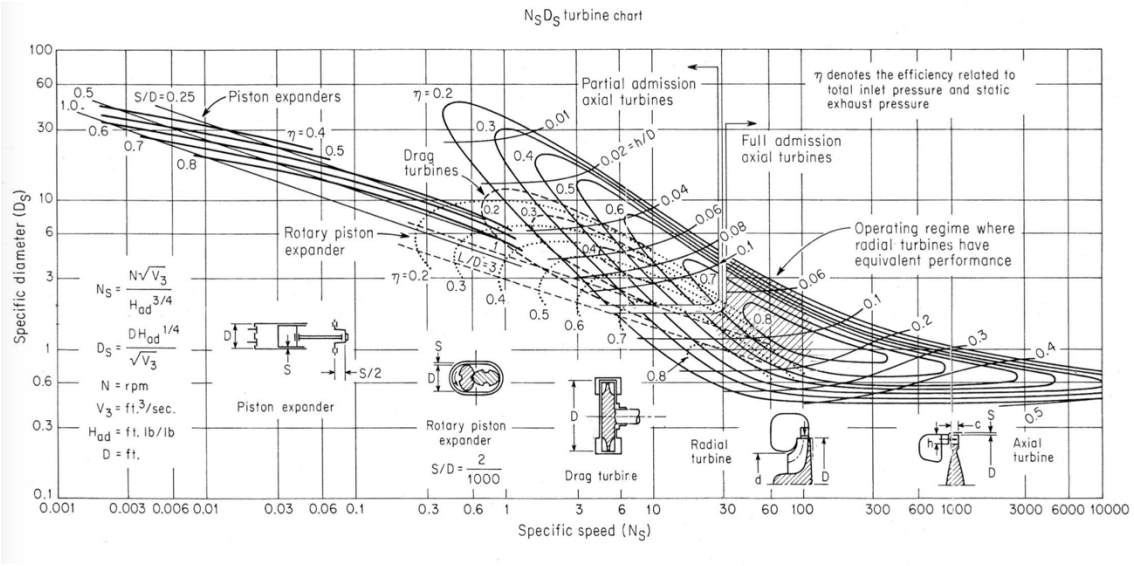

Figure 5. Piston Expanders Operate At A Much Lower Specific Speed Than Radial Turbines. Source: [12].

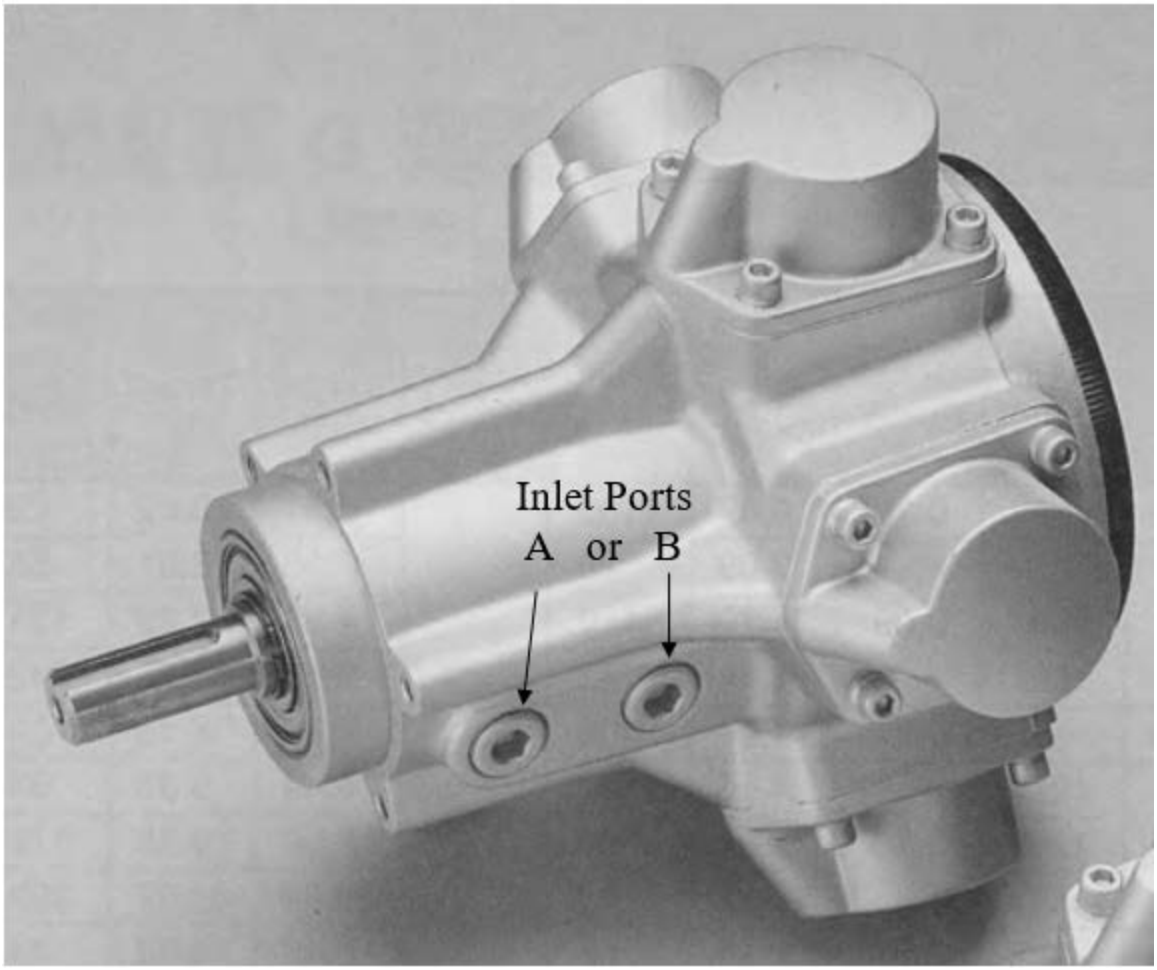

Figure 6. UTAM4-030 Radial Air Motor. Source: [5].

This motor is available with direct or geared drive, with a prescribed maximum operating pressure of 625 kPa (90 PSIG). It is fully reversible, with direction of turn dependent on the port used to input the air. Air enters the motor along the side of the motor, through either Port A or Port B (Figure 6), and goes along the shaft to the top of the cylinder (see cutaway in Figure 7), cycling the piston down and pushing the air out of the other cylinders. Each cylinder has only one opening that serves as air inlet and outlet, thereby prohibiting mixing of the air as it enters/leaves the cylinder. There are no valves or cam shaft associated with this motor, limiting the number of moving components. Air flow into and out of a cylinder was modeled in ANSYS Fluent, discussed further in Chapter V. Additional operating curves and parameters for the UTAM4-030 can be found in Appendix A. UTAM4-030 Operating Curves.

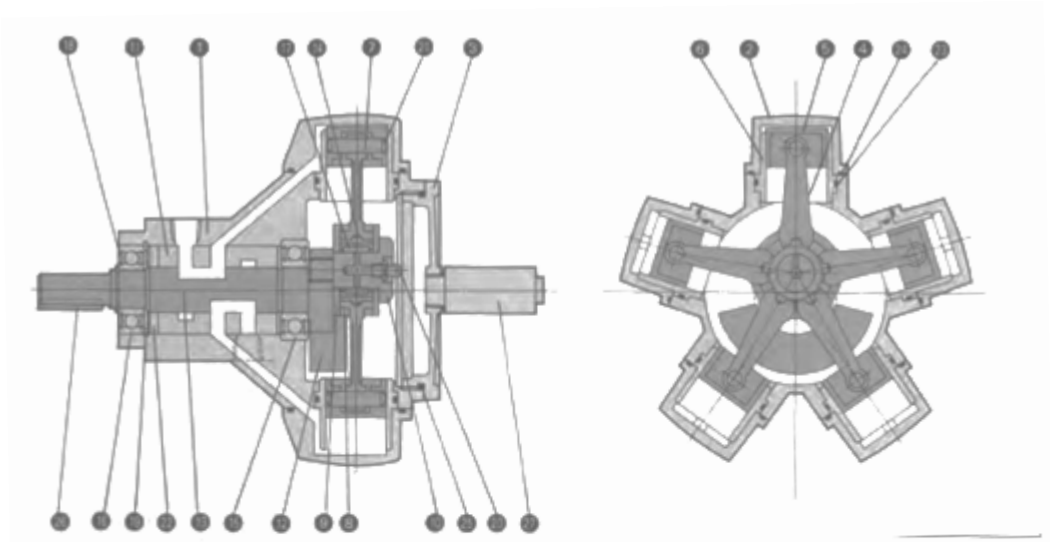

PARTS LIST

No.	Name	Material	Q'ty
●	Casing	Aluminum alloy	1
●	Cylinder cover	Aluminum alloy	3 (5)
●	End cover	Synthetic resin	1
●	Connecting rod	Aluminum alloy	3 (5)
●	Piston	Brass casting	3 (5)
●	Sleeve	Cast iron	3 (5)
●	Piston pin	Carbon steel	3 (5)
●	Ring	Carbon steel	2
●	Thrust washer	Carbon steel	2
●	Crank pin	Carbon steel	1
●	Valve bushing	Cast iron	1
●	Balance weight	Carbon steel	1
●	Shaft	Chrome molybdenum steel	1
●	Liner	Synthetic resin	3 (5)

No.	Name	Material	Q'ty
●	Bearing	—	1
●	Bearing	—	1
●	Needle bearing	—	1
●	Snap ring	—	1
●	Snap ring	—	1
●	Grease nipple	—	1
●	Copper rivet	—	1
●	Oil seal	N.B.R.	1
●	Gasket	N.B.R.	3 (5)
●	Gasket	N.B.R.	3 (5)
●	Gasket	N.B.R.	1
●	Key	—	1
●	Muffler	—	1

(●) Q'ty is for UTAM4-30.

Figure 7. UTAM4-030 Cutaway with Parts List. Source: [5].

Due to the low torque imposed by the initial AC Generator on the air motor, it was operated outside of the data curves provided by the manufacturer. The curves had to be extended to account for the operating range. Figure 8 and Figure 9 show the extended operating curves for Power and Torque of the UTAM4-030 Air Motor. To extend the curves, MATLAB was used to plot the existing curves through data selection, with a second order polynomial fit function applied to extend the curves.

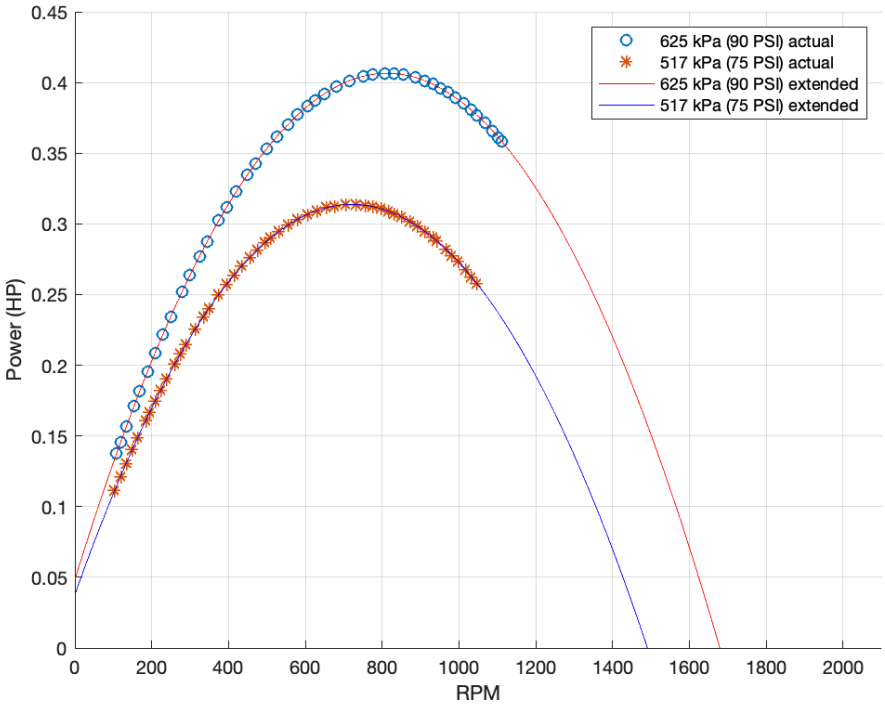

Figure 8. UTAM4-030 Power Curves

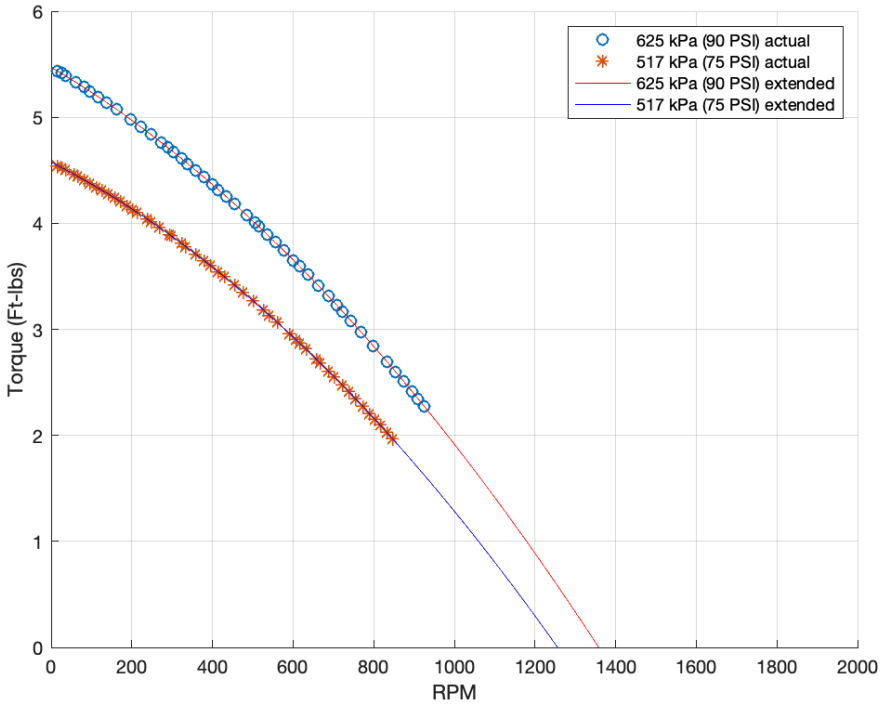

Figure 9. UTAM4-030 Torque Curves

Additionally, air supplied was above the rated 625 kPa (90 PSI) maximum, at 723 kPa (105 PSI). Air consumption curves had to be derived from the existing data for the 207 (30 PSI) through 625 kPa (90 PSI) curves using a MATLAB script to choose graph points to determine slope and intercepts. The data was recorded in an Excel file (Table 2) with the difference between the curve points for each RPM averaged and the air consumption for an RPM range of 0 to 2000 was developed for 625 kPa (90 PSI). All air consumption lines were the plotted together (Figure 10).

Table 2. Reference Data for Air Consumption At Various Air Pressures. Adapted from [5].

SCFM REFERENCE TABLE (105 SCFM Derived from averaged difference)							
RPM	105 PSI	90 PSI	75 PSI	60 PSI	45 PSI	30 PSI	Avg Delta
0.00	1.16	1.17	1.16	1.18	1.22	1.18	0.00
100.00	5.18	4.52	2.70	2.41	2.14	1.90	0.66
200.00	7.13	6.23	4.24	3.65	3.07	2.62	0.90
300.00	9.08	7.93	5.78	4.88	3.99	3.35	1.15
400.00	11.03	9.64	7.32	6.11	4.92	4.07	1.39
500.00	12.98	11.34	8.85	7.35	5.84	4.80	1.64
600.00	14.93	13.05	10.39	8.58	6.77	5.52	1.88
700.00	16.88	14.75	11.93	9.82	7.69	6.24	2.13
800.00	18.83	16.46	13.47	11.05	8.62	6.97	2.37
900.00	20.78	18.16	15.01	12.28	9.54	7.69	2.62
1000.00	22.73	19.87	16.55	13.52	10.47	8.42	2.86
1100.00	24.68	21.57	18.08	14.75	11.39	9.14	3.11
1200.00	26.63	23.28	19.62	15.98	12.32	9.87	3.35
1300.00	28.58	24.98	21.16	17.22	13.24	10.59	3.60
1400.00	30.53	26.69	22.70	18.45	14.17	11.31	3.84
1500.00	32.48	28.39	24.24	19.68	15.09	12.04	4.09
1600.00	34.43	30.10	25.78	20.92	16.02	12.76	4.33
1700.00	36.38	31.80	27.32	22.15	16.94	13.49	4.58
1800.00	38.33	33.51	28.85	23.39	17.87	14.21	4.82
1900.00	40.28	35.21	30.39	24.62	18.79	14.94	5.07
2000.00	42.24	36.92	31.93	25.85	19.72	15.66	5.32

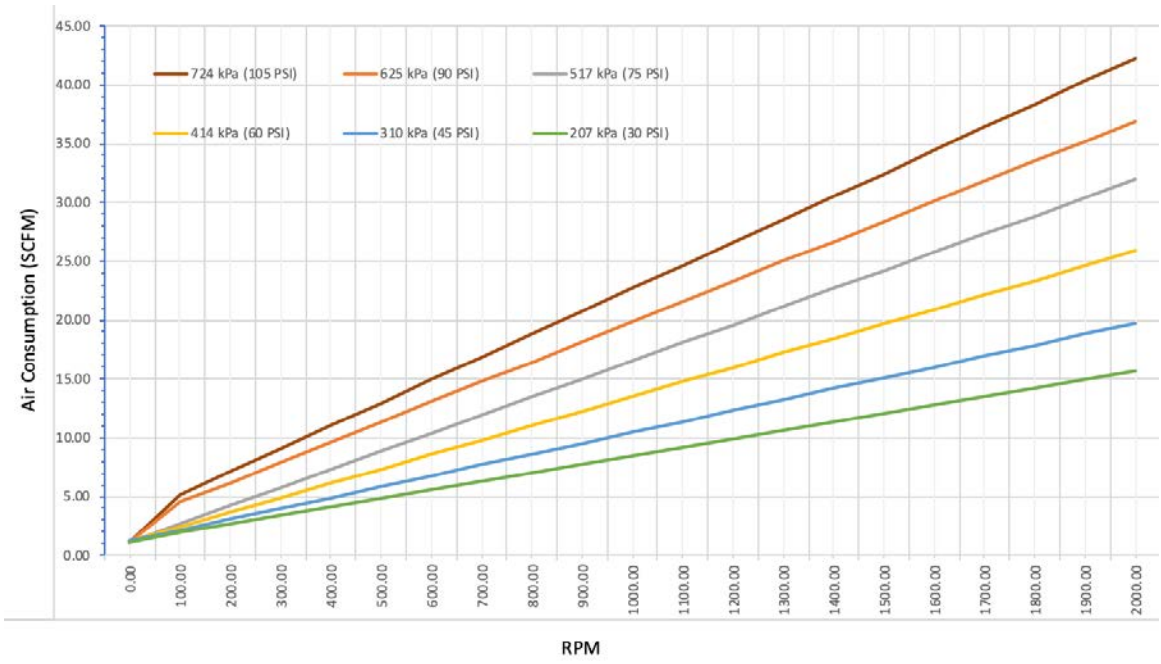

Figure 10. Air Consumption for Various Inlet Air Pressures with RPM

B. PERMANENT MAGNETIC MOTORS (GENERATORS)

Two different permanent magnetic motors were repurposed as permanent magnetic generators (PMGs). A PMG works through simple generator motion with a relative motion between a conductor and a permanent magnet, generating alternating current (AC). This type of generator is widely used due to the simple operation. The two models used for this research were the 150 KV rated three phase motor from Scorpion and the 80 KV rated three phase motor from XOAR. The ratings for each motor indicated RPM per Volt. PMGs were mounted directly to the shaft of the air motor, allowing for direct drive. To determine basic output of the PMG, a base of 900 RPM for the air motor was assumed. Given this, the RPM was divided by the KV rating of the PMG to determine voltage output using Equation (1a).

$$Voltage = \frac{RPM}{KV\ Rating} \tag{1a}$$

1. 150 KV Scorpion

The SII-6530-150KV Motor, shown in Figure 11, is a high efficiency electric motor typical of those used by RC airplane hobbyists. This motor has 12 stator arms with 14

magnetic poles. The maximum continuous current is 95 Amps with a motor resistance of 0.032 Ohms. Maximum continuous power is 4220 Watts. As the shaft size is M8x1.0, a flexible coupling has to be used to transfer the rotary motion from the air motor shaft to the generator shaft. For the 150 KV PMG, the output at 900 RPM was calculated to be 6 Volts using Equation (1b), allowing for the use of the ten times transformers to increase the voltage to above the voltage of the capacitor

$$6\,Volts = \frac{900\,RPM}{150\,RPM/Volt} \tag{1b}$$

Source: https://www.redwingrc.com/SCORPION-SII-6530-150KV-Motor-for-Giant-Scale-Airplane.html

Figure 11. Scorpion 150 KV Motor

2. 80 KV XOAR

The XOAR 80 KV motor, shown in Figure 12, is a high efficiency electric motor, also typical of the RC airplane hobby, used in applications that require high thrust to weight ratios. This motor has 12 stator arms with 18 magnetic poles. The maximum continuous current is 35.6 Amps with a motor resistance of 0.122 Ohms. Maximum continuous power is 1708.8 Watts. The shaft on the XOAR is hollow, with a hub connection, allowing for a coupler to be attached using screws. A hub to air motor shaft was designed and constructed using additive manufacturing to transfer the rotary motion from the air motor shaft to the generator shaft. The solid model is shown in Figure 13. Further discussion of the 3D printed coupling device is in Chapter IV, with a technical drawing in Appendix B. 3D Printed Coupling Device For the 80 KV PMG, the voltage output at 900 RPM was calculated to be 11.25 Volts. Combined with the ten times transformers, the output voltage of the system would be nearly double the voltage of the capacitor using Equation (1c).

$$11.25\ Volts = \frac{900\ RPM}{80\ RPM/Volt} \tag{1c}$$

Source: https://www.xoarintl.com/brushless-electric-motors/titan-air/titan-air-TA110-light-weight-pro-series/#spec

Figure 12. XOAR Titan Air 80 KV Motor

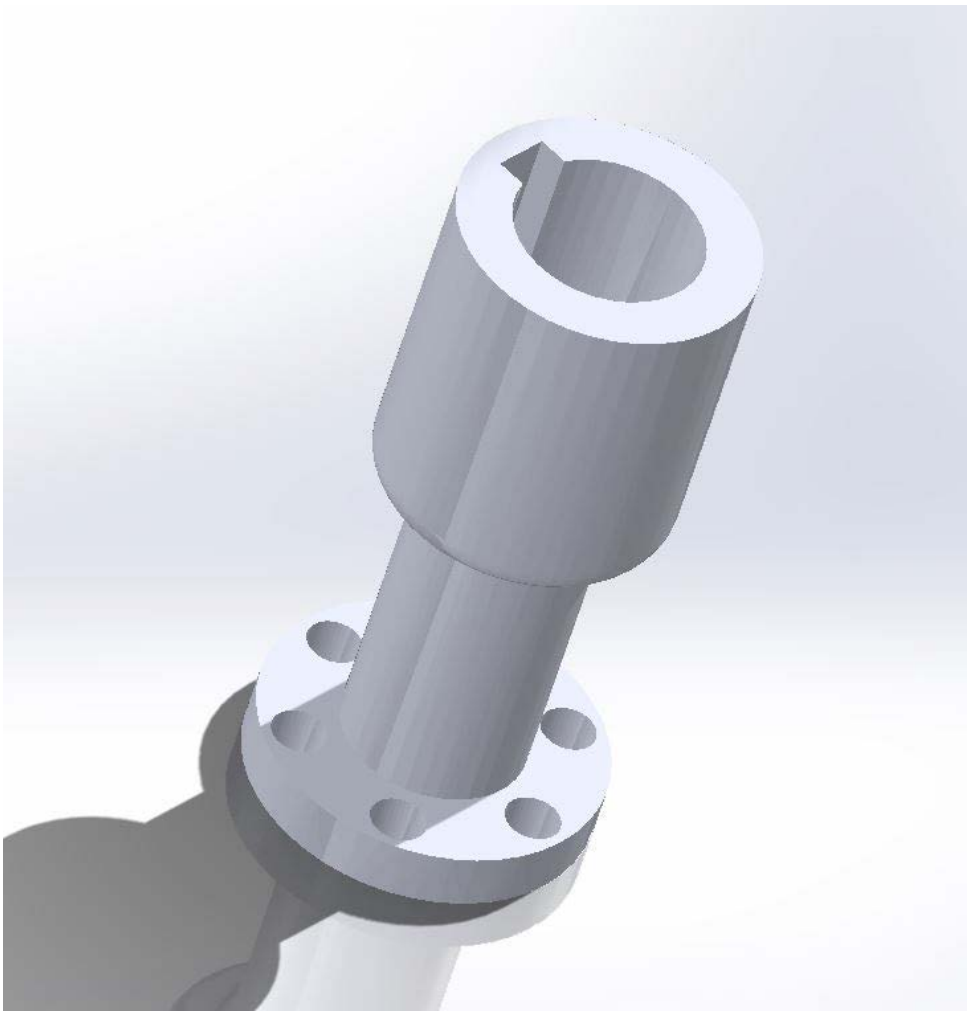

Figure 13. Solid Model Of Hub Assembly for the 80 KV PMG

THIS PAGE INTENTIONALLY LEFT BLANK

III. SYSTEM SETUP AND TESTING

Due to the similarities between the 150 KV and 80 KV setups, both can be described simultaneously with the minor differences annotated for the 80 KV PMG. All components, with the exception of the PMGs and the couplings, were identical throughout all experiments.

The radial air motor was mounted horizontally with a flange type mounting bracket to a mounting plate. The 150 KV PMG was mounted inside of an aluminum shell that allowed for three axis alignment of the shaft. The shaft of the PMG and the shaft of the air motor were aligned visually with a friction type flexible coupling uniting the shafts. The 80 KV PMG was mounted on a vertical plane, with the hub of the PMG towards the shaft of the air motor. Since the 80 KV PMG does not have a shaft protruding from the assembly in the conventional sense, a coupling was designed and made using additive manufacturing techniques to unite the shaft of the air motor to the hub of the 80 KV PMG. A detailed breakdown of the coupling design is seen in Appendix B.

Each phase wire of the PMGs was wired to three separate single-phase Emerson E200EWA transformers to increase the voltage of each phase by a factor of 10. Ratings for the transformers are in Table 3 with an example of the transformer in Figure 14 [6]. These stepped up phases were sent to the individual inputs of a MSD100-12 three phase rectifier [7]. The DC output voltage was wired directly to a 130 Farad, 56 V super-capacitor, pictured in Figure 15, for charging [8].

Table 3. Transformer E200EWA Ratings. Adapted from [6].

VA	Primary Fuse Holder Class "CC"			Dimensions						
	W Option – Midget Type Catalog Number	WA Option – Type 3AG w/ Covers Catalog Number	WB Option – Midget Type w/ Covers Catalog Number	Height in (mm)	Width in (mm)	Depth in (mm)	Mtg Width W1 / W2 in (mm)	Mtg Depth D1 / D2 in (mm)	Slot Size S1 / S2 in (mm)	Approx. Ship Weight lbs (kg)
50	E050EW	E050EWA	E050EWB	4.18 (106.2)	3.01 (76.5)	3.99 (101.3)	2.51 / N/A (63.8 / N/A)	2.02 / N/A (51.3 / N/A)	.20 x .33 / .20 x .33 (5.1 x 8.4 / 5.1 x 8.4)	3.0 (1.36)
75	E075EW	E075EWA	E075EWB	4.41 (112.0)	3.39 (86.1)	4.36 (110.7)	2.81 / 2.50 (71.4 / 63.5)	2.10 / N/A (53.3 / N/A)	.20 x .50 / .20 x .50 (5.1 x 12.7 / 5.1 x 12.7)	4.0 (1.82)
100	E100EW	E100EWA	E100EWB	4.41 (112.0)	3.39 (86.1)	4.61 (117.1)	2.81 / 2.50 (71.4 / 63.5)	2.37 / N/A (60.2 / N/A)	20 x .50 / .20 x .50 (5.1 x 12.7 / 5.1 x 12.7)	5.0 (2.27)
150	E150EW	E150EWA	E150EWB	5.36 (136.1)	4.50 (114.3)	4.48 (113.8)	3.74 / 3.12 (95.0 / 79.3)	2.56 / 2.87 (65.0 / 72.9)	.20 x .65 / .20 x .33 (5.1 x 16.5 / 5.1 x 8.4)	8.0 (3.64)
200	E200EW	E200EWA	E200EWB	5.36 (136.1)	4.50 (114.3)	4.79 (121.7)	3.74 / 3.12 (95.0 / 79.3)	2.87 / 3.18 (72.9 / 80.8)	.20 x .65 / .20 x .33 (5.1 x 16.5 / 5.1 x 8.4)	10.0 (4.55)
250	E250EW	E250EWA	E250EWB	5.36 (136.1)	4.50 (114.3)	5.21 (132.3)	3.74 / 3.12 (95.0 / 79.3)	3.29 / 3.61 (83.6 / 91.7)	.20 x .65 / .20 x .33 (5.1 x 16.5 / 5.1 x 8.4)	11.0 (5.00)

Adapted from https://www.emerson.com/documents/automation/catalog-solahd-sbe-series-transformers-en-us-163796.pdf

Figure 14. Emerson E200EWA Transformer (center). Source: [6].

Figure 15. Maxwell 56V 130 Farad Super-capacitor. Source: [8].

Several data collection points were established to quantify and monitor the equipment during operation. The voltage of the super capacitor was measured at the positive and negative direct current (DC) terminals of the rectifier where the wires were connected to the super-capacitor. The capacitor voltage was then fed into a DC transducer to convert the voltage into a 0 to 10 volts signal, that was sampled by a USB Multifunction I/O DAQ, pictured in Figure 16. A tachometer was installed on the side of the box enclosing the motor-generator apparatus to measure the speed of the rotating generator. This signal was fed to a digital read out for the operator and also input to the NI DAQ. The signals from the NI DAQ were read by MATLAB for plotting and data collection. Pressure data was collected from the input of the air motor with an air sensing line to a pressure scanner that sent pressure data via ethernet cable to the computer, read by MATLAB.

Figure 16. National Instruments Multifunction DAQ, Model USB-6003 16 Bit. Source: [9].

All data was input directly into MATLAB with a real time graph plotting voltage, current, power, air pressure, and RPM. Additional code was used post process the graphs to eliminate the noise that was plotted. Code used for post-processing and individual plotting is available in Appendix C. MATLAB Code used to plot data from run figures and the data collection code is available in Appendix D. MATLAB Code used to record data from each run

IV. RESULTS

Both system setups were tested with air directly from an air reservoir with pressure maintained by a running air compressor, with air pressure dropping no more than 3 PSI during operations. The 150 KV PMG was ran at an inlet pressure of 517 kPa (75 PSI) with the 80 KV PMG ran at 620 kPa (105 PSI). These were different due to the air supply systems connected. The 80KV PMG runs were conducted on the same air supply as Pelletier [4] in order to standardized air supply. The 150 KV PMG was ran on a different air supply with a slightly lower volume, leading to increased cycling from the air compressor. Results for both were compared to establish the most air efficient set up. Both motors were tested to establish the charge time required to bring the 130F/56 Volt Maxwell Super-capacitor to 56 Volts from a completely discharged state. Time, RPM, capacitor voltage, current, and power were recorded for each data collection run. The only differences between each set up were the KV PMG used as the generator. As capacitor voltage was measured, current and power were derived from the capacitor voltage level. Current was calculated, using Equation (2), as the change in voltage over the change in time, or *dv/dt*, multiplied by the capacitance of 130 Farads. The resultant calculated current was multiplied by the voltage, using Ohm's Law, to determine power using Equation (3). Both of these functions were programed into MATLAB to instantaneously plot voltage, current, and power versus time. The code is available in

$$\mathrm{I} = \mathrm{C}\frac{dv}{dt} \tag{2}$$

$$P = I \times V \tag{3}$$

Equation. (4) was used to calculate capacitor energy in Joules using the capacitance and the maximum voltage that it was charged. Equation (5) was used to determine mass, in kilograms, per second, using the standard density of air (ρ =1.225 kg/m^3) and the instantaneous mass flow rate (Q). The air pressure ratio across the air motor was used in Equation (6) to calculate the outlet temperature. These were combined in Equation (7), along with the specific heat capacity of air, 1004 J/kg-K, to determine the amount of energy

used by the system. The energy of the capacitor was divided by the energy into the system to determine overall efficiency in Equation (8).

$$E_{cap} = \frac{1}{2}CV^2 \tag{4}$$

$$mass\ (m) = \rho Q \tag{5}$$

$$T_2 = T_1\left(\frac{P_2}{P_1}\right)^{\frac{\gamma-1}{\gamma}} \tag{6}$$

$$E_{in} = mc_p(T_1 - T_2) \tag{7}$$

$$\eta = \frac{E_{cap}}{E_{in}} \tag{8}$$

A. 150 KV PMG RESULTS

The selection of the 150 KV PMG was based upon a low KV rating when compared to the ones used in previous work. With the turbocharger set ups, KV ratings of 560 and 520 were used [3,4]. These PMGs were small, did not require substantial amounts of torque, and worked well at high RPM, ideal for use with the turbocharger. For the air motor that would be operating at an RPM range much lower than the turbochargers, a lower KV rating would be required to generate sufficient voltage to charge the 56 V/130 F capacitor. 840 RPM was required to generate a minimum of 5.6 volts (stepped up to 56 Volts with the transformers to match the super-capacitor rating) with the 150 KV PMG, which is directly at the peak of the operating band of the air motor. Installation of the 150 KV PMG faced the main challenge of the coupling device as the shaft on the air motor was larger than the shaft of the 150 KV PMG, 16mm for the air motor and 8mm for the 150 KV PMG. A commercially procured friction type flex coupling was used with an improvised shaft key.

During operation, the air motor was found to be over powered for the use with the 150 KV PMG. RPM during operation ranged from 1200 at start and 1800 at the end of the charge cycle, well outside of the operating curves provided by the manufacturer. The RPM signal input was very noisy, with data drops shown without an actual change in RPM, likely

caused by environmental electromagnetic noise. The orange line in Figure 17 is the noise free, cleaned up data line showing the actual RPM. To clean up the data, the low points were deleted and replaced with a linear interpolation on from a data point on either side of the data point. The steep increase at 100 seconds was due to fully opening the inlet valve. Initial throttling of the inlet was done to verify system response and limit initial current spikes. The dips in the curve are representative of the compressor cycling to maintain air pressure.

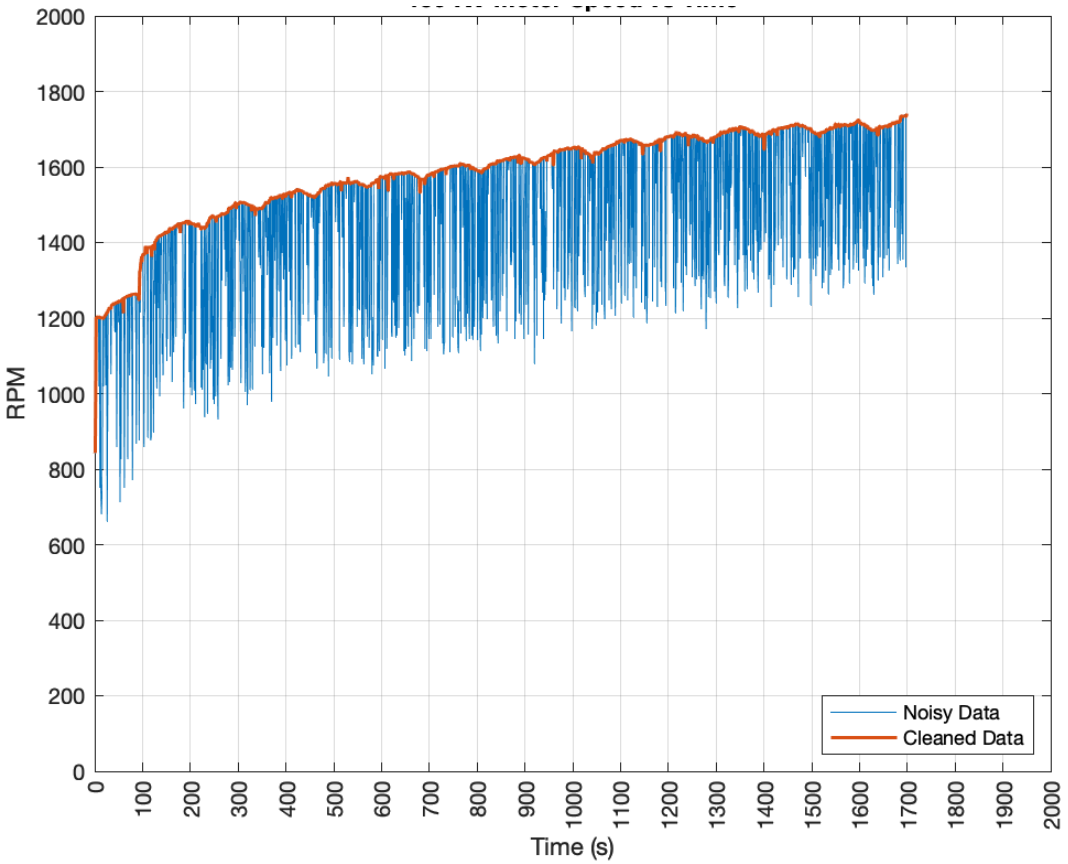

Figure 17. RPM versus Time (s) for the 150 KV PMG

Current and power curves were as expected when charging a super capacitor, with a very high initial current that develops into an exponential decay curve, typical of charging a completely discharged capacitor. Both curves were derived directly from the capacitor voltage plot, resulting in noisy data as well (Figure 18 and Figure 19). Peak current was

observed to be at 18 Amps then steadying out around 2–3 Amps during the majority of the charging cycle. Initial power began at approximately 40 Watts (0.05 HP), steadily climbing to and steadying out at 120 Watts (0.16 HP).

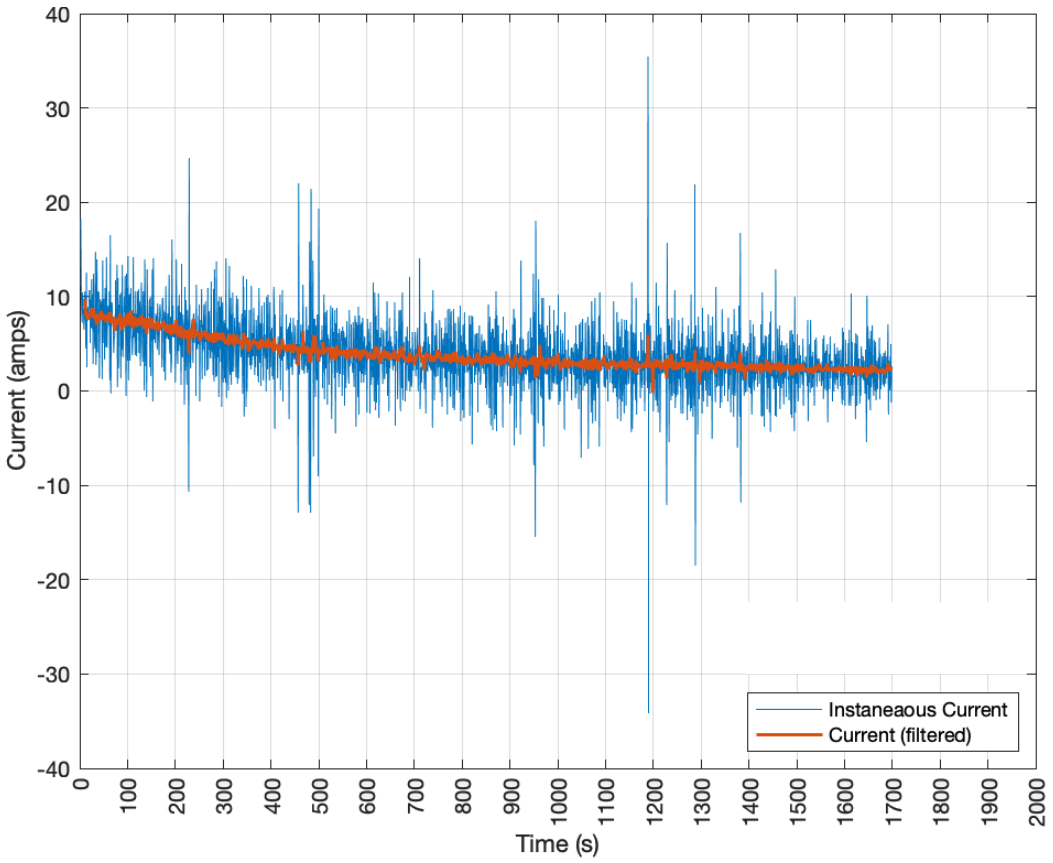

Figure 18. Filtered and Raw Current Data Versus Time, Instantaneous In Blue And Filtered In Orange, 150 KV PMG

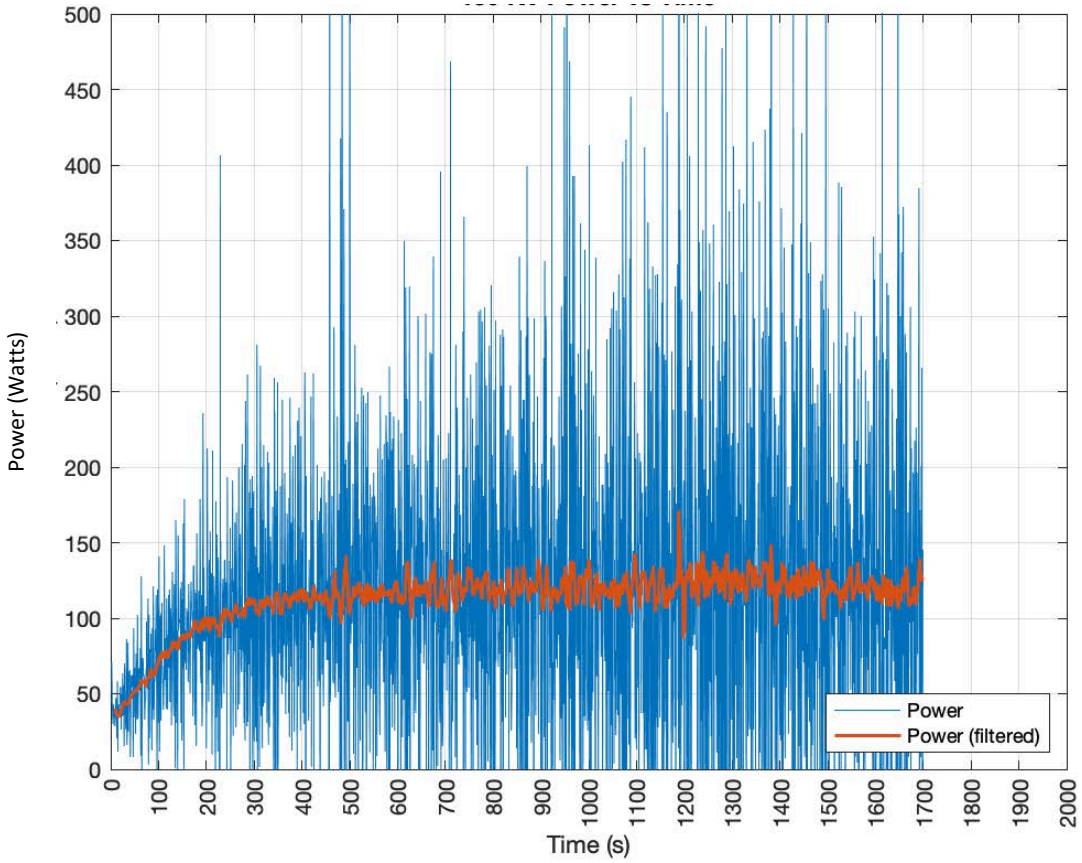

Figure 19. Filtered and Raw Power Data for the 150 KV PMG

All charging cycles were analyzed to determine the total volume of air consumed. The SCFM usage varies with RPM and was approximately 20.5 cubic meters (723.5 SCF) of air over the entire charge period, a decrease of nearly 50% air mass consumed over the turbocharger (with air ejector) for the same super-capacitor, even with the charge time taking 77% longer at 1700 seconds (28.3 minutes). Pelletier's work with the turbocharger used a constant 3214 cubic meters per min (90 SCFM) for 960 seconds (16 minutes), resulting in an air usage of approximately 51,428 cubic meters (1456 SCF) of air [4]. Figure 20 shows the voltage versus time. This curve was used with the air consumption curves to determine air mass consumed during the charge period. This lower power demonstrated the increased efficiency of the radial air motor over the automotive turbocharger with lower energy consumption, proving the viability of the radial air motor as a prime mover. Efficiency of the radial air motor with the 150 KV PMG was 7.5%.

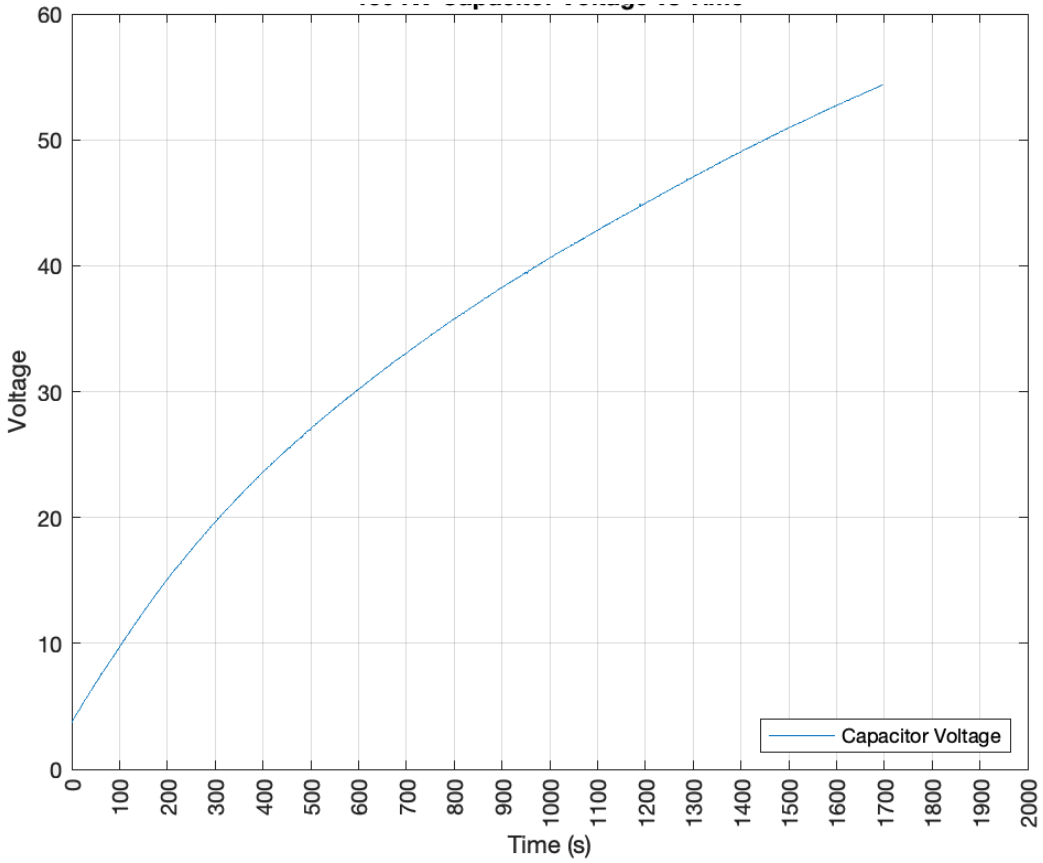

Figure 20. Capacitor Voltage versus Time (150 KV PMG for the Maxwell 56 V/ 130 F Supercapacitor)

Tests at a higher inlet pressure were not conducted because this would have substantially increased the RPM, posing a potential safety risk from failure of the air motor. This was able to charge the 56 V/130 F capacitor in approximately 28 minutes at 517 kPa (75 PSI) inlet pressure. The decision was made to decrease the KV rating and use an 80 KV PMG to bring the air motor speed down, closer to the manufacturer operating parameters.

B. 80 KV PMG RESULTS

The 80KV PMG was tested with two coupling devices, both of identical geometry but made from different materials. The first coupling device (additive manufactured PLA) required a cooling line from the discharge of the air motor, creating a flow restriction. The

second, additive manufactured 17–4 Stainless Steel, required no flow restrictions on the outlet of the air motor.

1. PLA Coupling Device

Initial tests with the 80 KV PMG had heat generation on the PMG and hub that was sufficient to bring the coupling, when made from PLA, to the point of failure, shearing the hub connection from the coupler, shown in Figure 21. This failure prevented operation of the system to charges of more than 25 Volts. A cooling line was installed, using the discharge port of the air motor, to direct cool air exhausted from the air motor directly onto the coupling at the hub connection. This prevented failure from the heat generated by the operating 80 KV PMG. This cooling line created a back pressure condition with the outlet of the air motor, lowering the differential pressure across the air motor, resulting in a slower rotation. The extent of this reduction was not analyzed.

Figure 21. Failed PLA Coupling Device

Once a solution to the heating problem was found, testing was able to continue and charge the super-capacitor in 1400 seconds (approximately 23 minutes), while using approximately 11.2 cubic meters (396 SCF) of air. This cut the overall charge time down from the 150 KV PMG by 300 seconds (5 minutes), slightly decreasing the volume of air used and the time required to charge, and thereby increasing overall efficiency. This arrangement, due to the flow restriction on the outlet, turned at a much lower RPM than the other tests, allowing the air motor to run near peak power for the majority of the charging cycle. The RPM range observed was from 400 RPM to 900 RPM during operations, with RPM increasing as capacitor voltage increased. RPM data was calibrated to correct experimental/system bias, with 1000 added to the reading then dividing the sum by 2 (Figure 22). The flow restriction and the increased torque demand brought the running RPM well within the peak power range of the air motor.

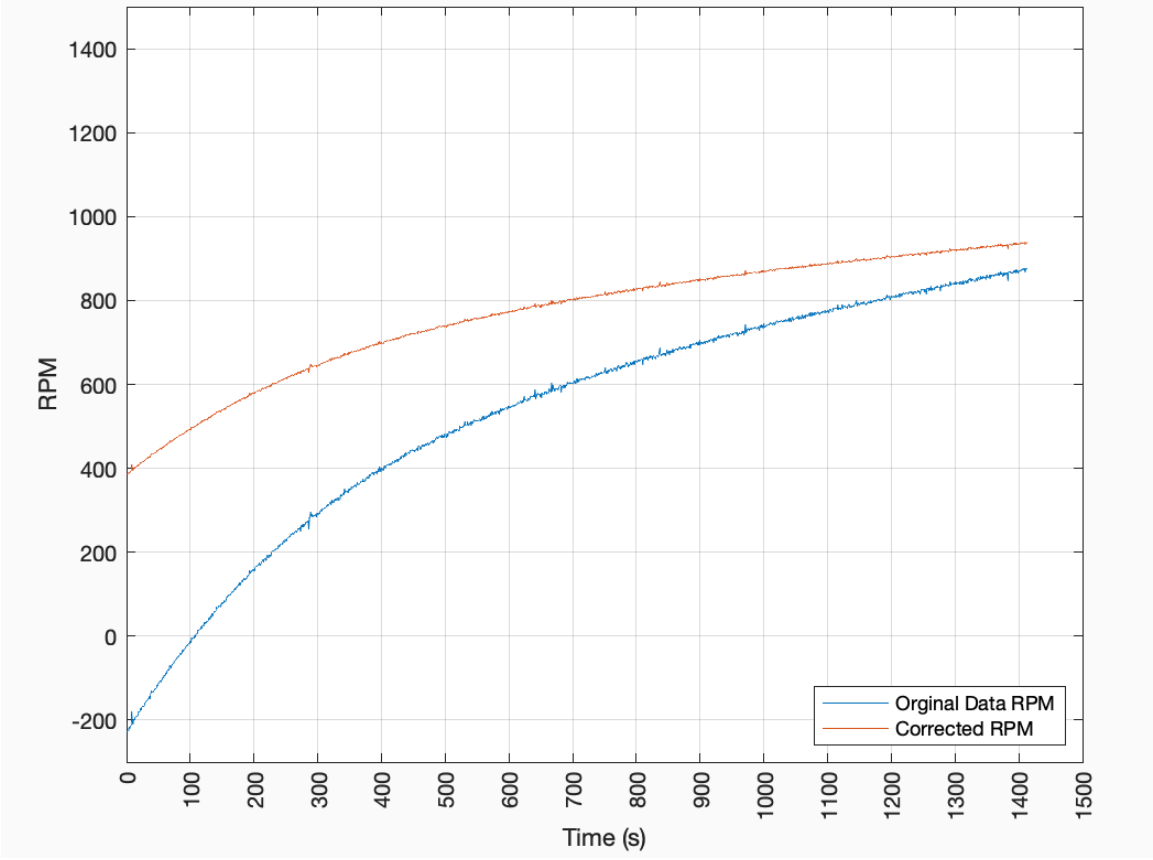

Figure 22. RPM versus Time for the 80KV PMG (with Flow Restriction)

The lower KV rating increased the overall performance through lower air mass consumed and a lower charging time. Higher current was observed over the range of operation, with a peak current of 25 Amps that settled out to 2–3 Amps (Figure 23). The 80 KV PMG was able to maintain a higher current at the beginning of the charge cycle, lowering the overall charge time.

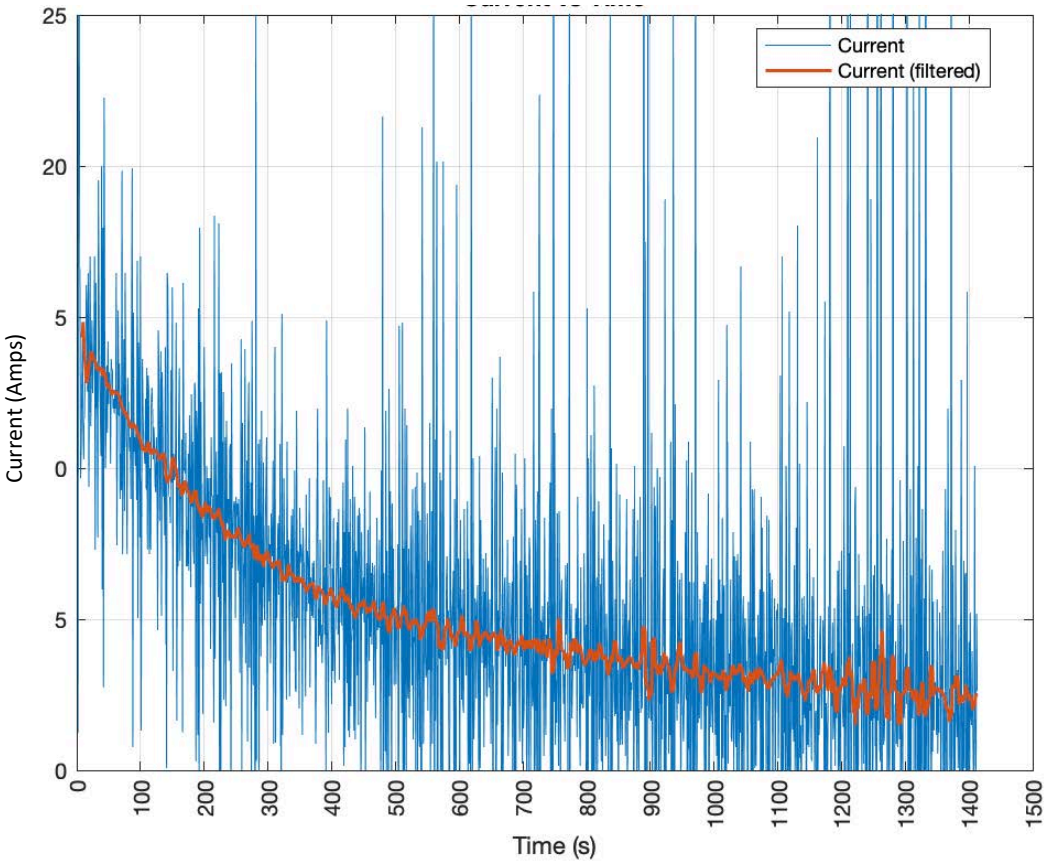

Figure 23. Current versus Time, 80 KV PMG (with Flow Restriction)

This increased current directly contributed to the increased the power. A peak power of 150 Watts (0.20 HP) that trended to 120 Watts (0.16HP) during the charge cycle was observed (Figure 24). The change out of the 150 KV PMG to the 80 KV PMG resulted in a higher efficiency of the system at 11.93% with the flow restriction attached, an increase of 4.4%.

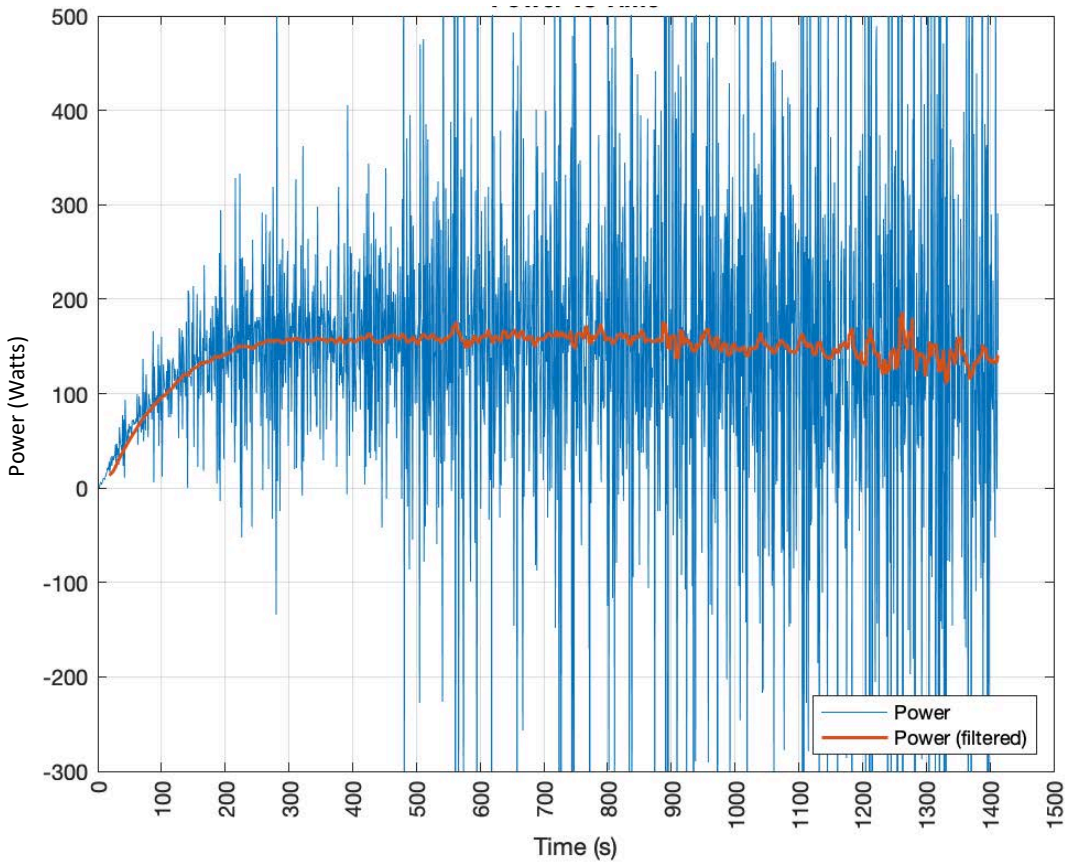

Figure 24. Power versus Time for the 80 KV PMG (with Flow Restriction)

2. 17-4 Stainless Steel Coupling Device

Another coupling device was additive manufactured from 17–4 Stainless Steel on a Desktop Metal 3D printer using the same solid model as the PLA. This printer works in a similar fashion to conventional plastic additive manufacturing processes with the raw material coming as bars that are drop loaded into the print head, heated, and extruded. The base material is 17–4 SS powder suspended in a binding matrix of plastic. The part is printed, then the binding agent removed. After the binding agent is removed, the now completely steel part has to be sintered in a furnace to remove the voids left behind. No additional post processing was required or conducted on the 17–4 SS coupler. Both couplers can be seen in Figure 25.

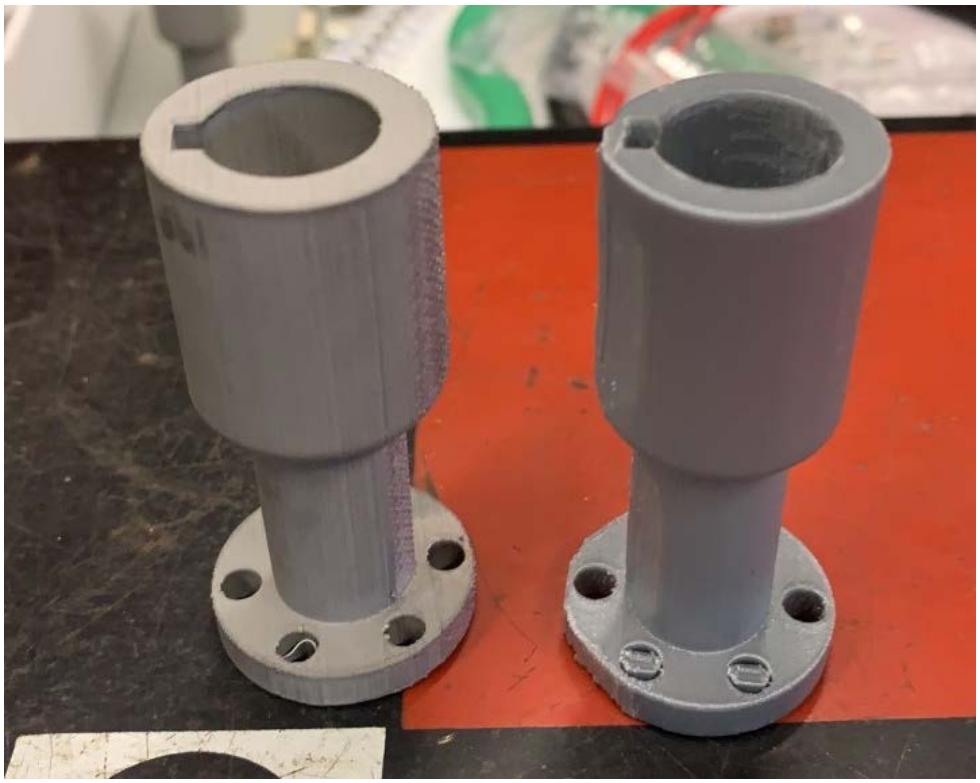

Figure 25. Additive Manufactured Couplings, 17–4 SS (left) and PLA (right)

The 17–4 SS coupler was not susceptible to failure at elevated temperatures. It allowed for system operation without the cooling line installed, bringing the operating rotation rate of the air motor to a range of 800 to 1400 during its use. Motor/generator rotation rate was expected to increase with the removal of the flow constriction on the discharge port. The observed “saw tooth” plot of the RPM corresponds to the cycling of the air compressor to maintain air pressure (Figure 26).

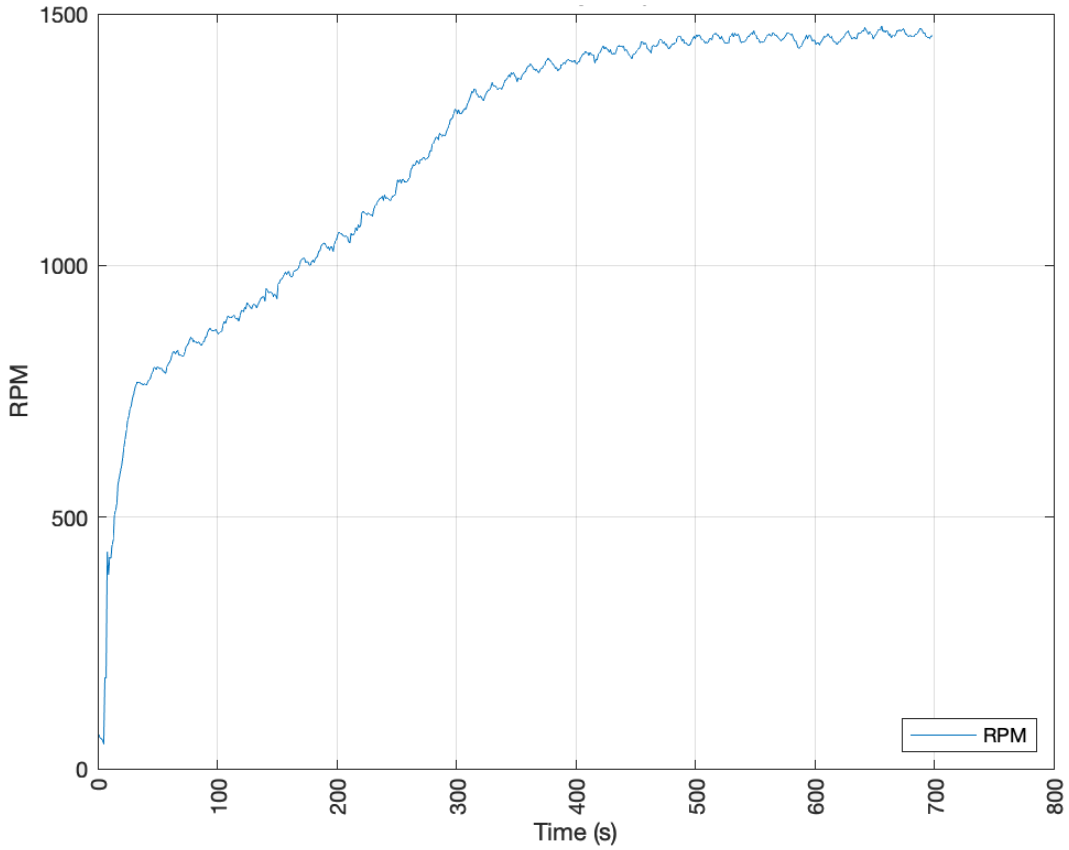

Figure 26. RPM versus Time for the 80KV PMG (without Flow Restriction)

The increase speed also increased the output voltage (and subsequently the current), bringing charge time down from 1400 seconds (23 minutes) to 700 seconds (11.6 minutes) from completely discharged to 56 Volts, using 8.6 cubic meters (305 SCF) of air. This brought the peak current to 22 Amps with current steadying out at 7 Amps (Figure 27), a two-fold increase over the same KV PMG with the flow restriction. This increased current was vital to bringing down the charge time.

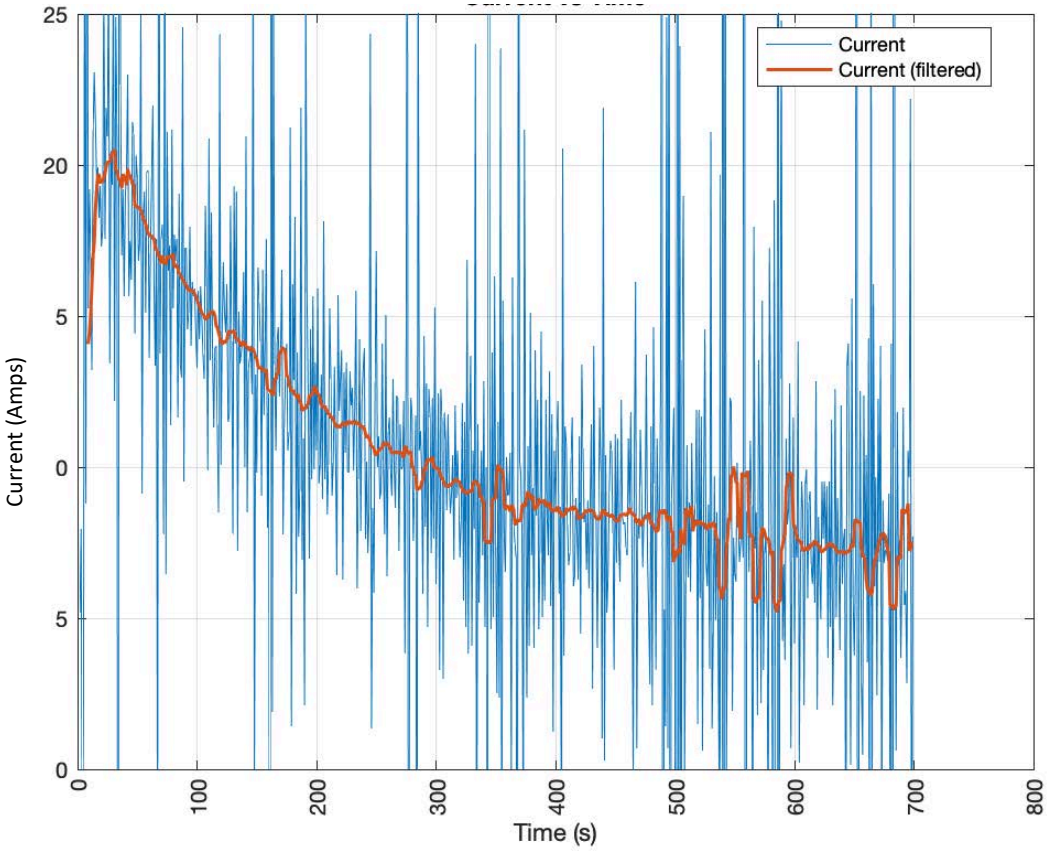

Figure 27. Current versus Time for the 80KV PMG (without Flow Restriction)

Subsequently, with a marked increase in current, the power output increased as well. Peak power output for the 80KV PMG, without the flow restriction, was higher than the rated power output of the air motor. The air motor was operating with an inlet pressure outside of the rated 625 kPa (90 PSI) at 723 kPa (105 PSI). Peak observed power was 383 Watts (.51 HP) with power steadying out at 360–380 Watts (0.48-0.51 HP) (Figure 28).

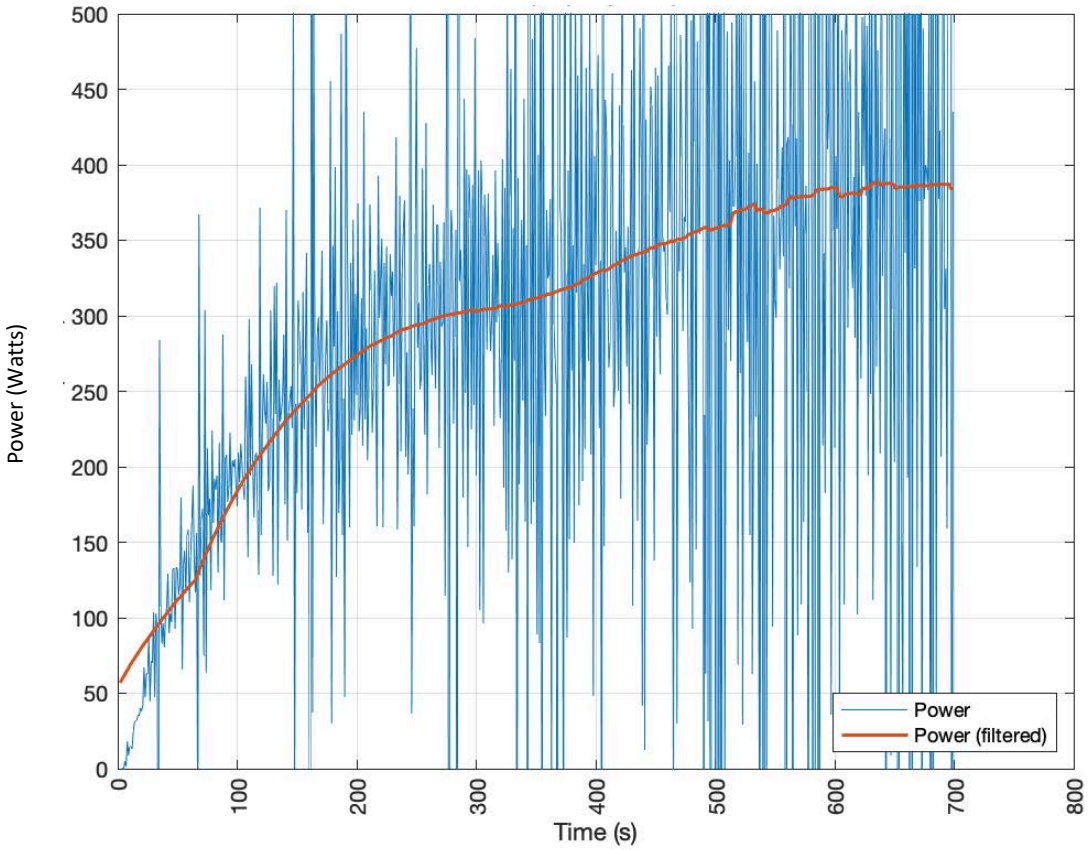

Figure 28. Power versus time for 80KV PMG (without Flow Restriction)

For comparison, the plots for all three charging cycles are shown combined in Figure 29. The improvements with the 80KV PMG (without the flow restriction) are readily apparent. The 150KV PMG, even with the capacitor starting at 3 Volts, still took over twice as long to charge the capacitor. The efficiency of the 80 KV PMG without the flow restriction took system efficiency to 15.5%, nearly double that of the 150 KV PMG. System efficiency of McLaughlin [3] and Pelletier [4] was 0.094% and 0.028% respectively for their final configurations. All efficiencies are shown in Table 4.

Table 4. Configuration Efficiencies

Configuration	Efficiency
Automotive Turbo (charging 16V/500F Capacitor) [3]	0.094%
Automotive Turbo (with air ejector) [4]	0.028%
Radial Air Motor with 150 KV PMG	7.54%
Radial Air Motor with 80 KV PMG (with flow restriction)	11.93%
Radial Air Motor with 80 KV PMG (without flow restriction)	15.48%

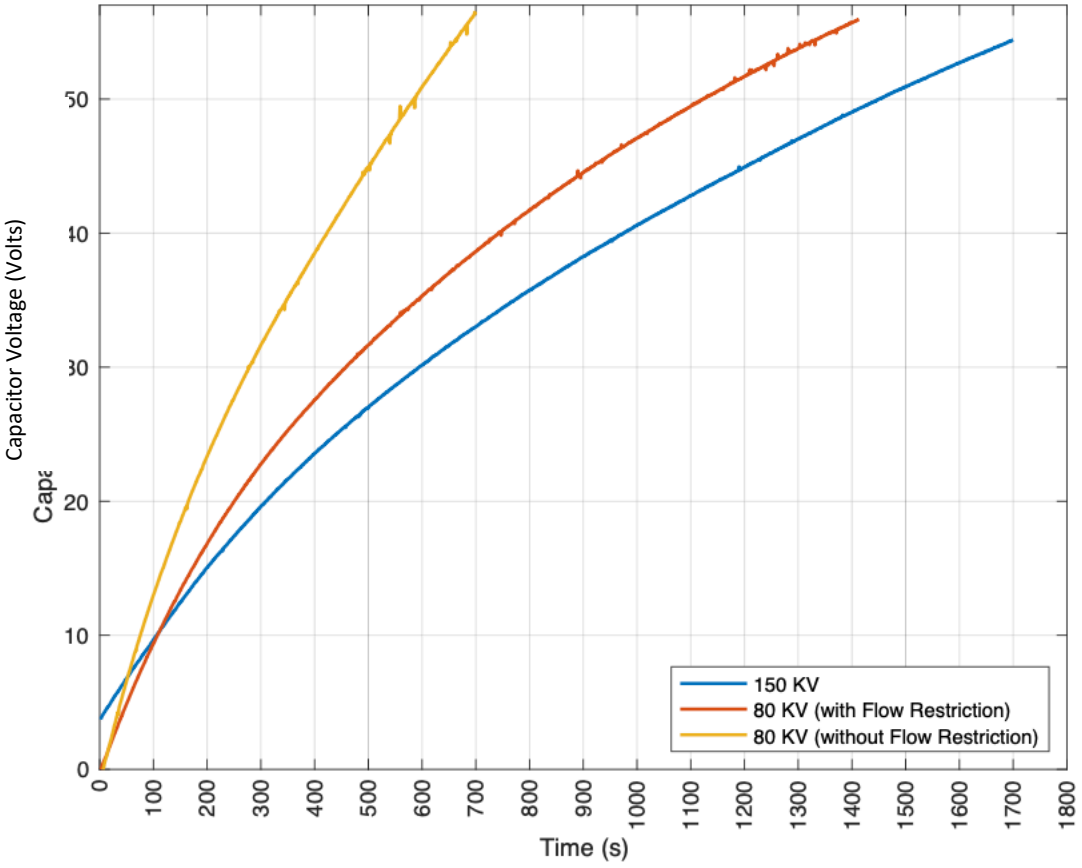

Figure 29. Combined Curves for All Three Charging Cycles

THIS PAGE INTENTIONALLY LEFT BLANK

V. ANSYS-FLUENT MODELING OF AIR MOTOR CYLINDER

The fluid flow into and out of one of the cylinders of the radial air motor was modeled in ANSYS Fluent. This allowed for a theoretical computation of air flow. The commercially available, off the shelf versions of this motor, come in three and five cylinder variants. The simulation broke analyzes a single cylinder in an effort to develop a design procedure for future air motor optimization. Fluent was used over CFX due to the intricacies and difficulties associated with transient flow and a reciprocating deforming mesh. CFX is best when used for steady state flow, though it does have some limited transient flow and deforming mesh capability. Using various tutorials, Fluent was used as it was best able to replicate the reciprocating action of the piston/cylinder action of the air motor.

A. SOLID MODEL PREPARATION

To begin the set-up of the ANSYS model, a solid model was developed. Using the cross sectional diagrams from the manual and actual measurements, a simplified solid model was built in SOLIDWORKS. To simplify the geometry, just the cylinder and piston head were used, with the filleted combined inlet and outlet port. The piston head of the physical air motor had a small machined out area that slightly increased surface area that was ignored and assumed flat for the model. The inlet/outlet passages leading up the cylinder and along the shaft of the air motor were not simulated to decrease the complexity of the solid model and decrease computational time. The dynamics of the interior of the air cylinder were the focus of the study. The geometry of the cylinder made for a control volume that has only one port for fluid to enter and subsequently exit the cylinder, thereby eliminating mixing of the in-flow and out-flow that is typically seen in reciprocating piston machinery that has separate ports for in-flow and out-flow. The flow port is located at the top of the cylinder, on the cylinder wall, above the upper most point of travel for the piston. Models of the cylinder and piston are shown in Figure 30. Dimensions used to construct the solid model are shown in Table 5.

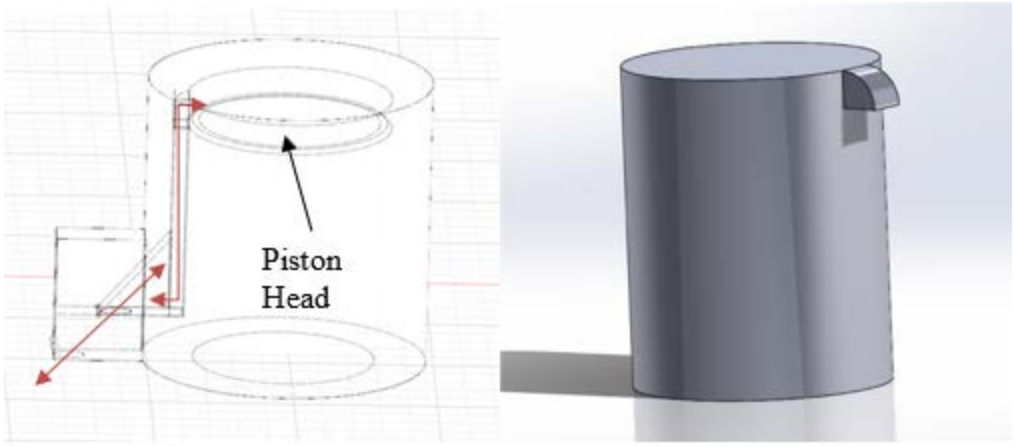

Figure 30. Left: Wireframe Model of Cylinder, Piston at Top. Flow Arrows in Red. Right: Solid Model of Cylinder, with In/Out Port Shown

While setting up the transient simulation, the solver required an input to dictate the motion of the piston within the cylinder. The solver uses text file input, with two rows each representing time and constant velocity respectively. The actual velocity curve of a reciprocation action is that of a sine wave. For this simulation, a constant velocity, alternating between positive and negative and corresponding to a periodic time scale, was used. This gives a triangular wave, providing a reasonable approximation the sinusoidal action for the purposes of simplifying computational time. Fluid properties used for the simulation was air at standard temperature and a pressure of 30 PSI (206 kPa), replicating compressed air being used as the driving fluid.

Table 5. Dimensions Of The Cylinder Used To Build Solid Model

Component	Piston Diameter	Cylinder Depth (at bottom of stroke)	Piston Travel	Port Width	Port Height	Port depth
Dimension (cm)	3.156 cm	3.5 cm	2.82 cm	0.5 cm	0.45 cm	0.5 cm

B. ANSYSY SET UP AND TRANSIENT MESHING

Named selections were created on the Piston Head, Cylinder Wall, Cylinder Head, and all sides of the inlet/outlet port. When building the mesh, no selections are made at that

point with regards to mesh deformation or body motion. This occurs in the solver Setup section of ANSYS Fluent. A “Medium” sizing was selected for the initial mesh and used for all subsequent simulations. When “Fine” was selected, negative cells volumes would occur while running the solver. Under “Quality,” a “Target Skewness” of $1x10^{-4}$ was used with all other selections left at default. A mesh refinement study was not conducted. The resulting final mesh had 374,121 Nodes and 270,528 elements. This gave a sufficiently refined mesh to adequately model the small volume of the interior of the cylinder. Figure 31 has the final mesh.

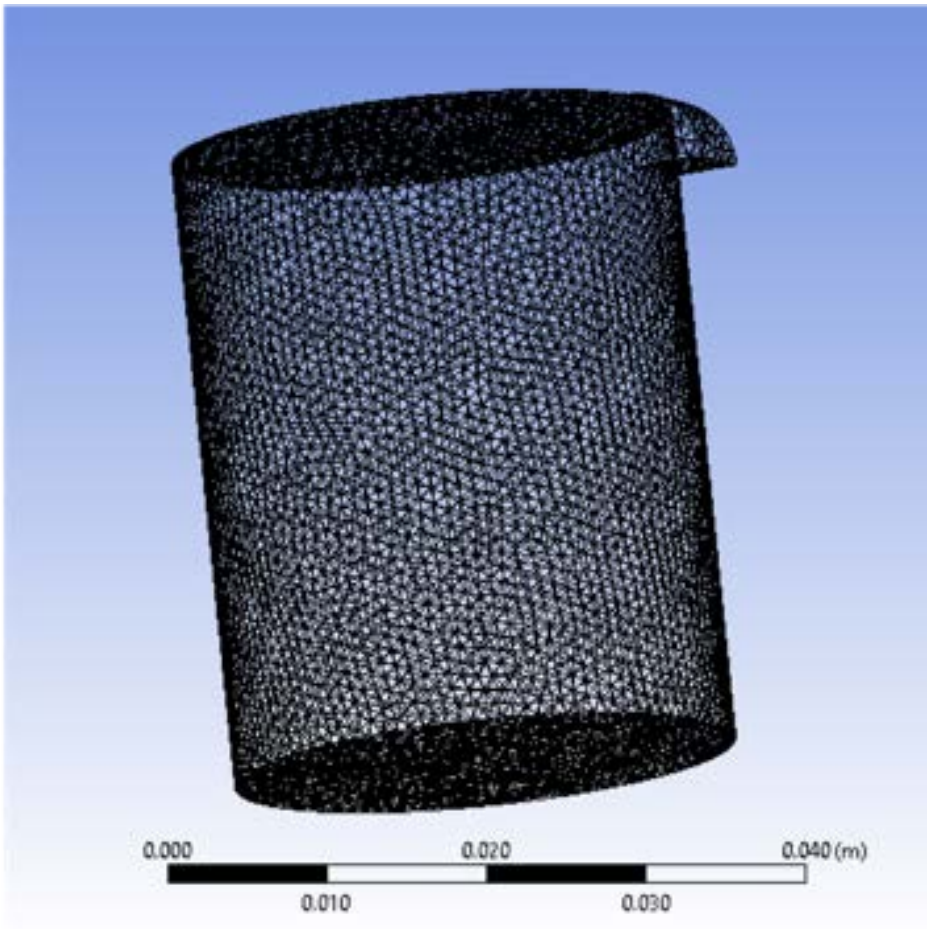

Figure 31. Final Mesh Used for ANSYS Fluent Simulation

To set up the solver, under the “general option,” “3D,” “Pressure Based” and, “Transient” were selected with, “Gravity,” turned on and set to -9.81 m/s on the Y-Axis.

The viscous flow model was selected using the standard k-Epsilon turbulence model with the energy equation enabled. Air at 25° C was selected as the working fluid and set to, "Ideal Gas," conditions for density. Failure to set air as an ideal gas for the solver resulted in failure of the solver from negative cell volumes.

Under "Boundary Conditions," the following named selections were set to "Walls": Cylinder Wall, Cylinder Head, Piston Head, and the sides of the Port. The port itself (the plane normal to the Y-Axis under the fillet) was set to "Inlet-Vent." This allows the working fluid to pressurize in and then flow out. A velocity profile was written in a text file for the piston head with a constant velocity associated with a time. For example, from time 0 to time 1, the piston could have a constant velocity of 2 m/s. To replicate the oscillation of the piston, the negative velocity was associated with time from 1–2. A "Dynamic Mesh" is then selected and set to "Smoothing" with "Diffusion" checked and a diffusion parameter of 2.

To cause the mesh deformation, creation of a dynamic mesh zone was required and the profiles for the piston motion and pressure have to be read, importing them into the solver. Dynamic Mesh was selected from the toolbar and the "Dynamic Mesh" box checked, enabling the setting of dynamic mesh zones. For this instance, dynamic mesh zones were required for the Cylinder Wall and the Piston Head. A dynamic mesh zone was created for the cylinder and set to "Deforming." For the geometry definition, it was changed from the default of "Faceted" to "In Cylinder," with the radius set to that of the radius of the cylinder. The axis of the cylinder defaults to the X-axis and has to be changed to reflect the axis of that the cylinder is actually on, which was the Y-Axis for this. A "rigid body" deforming mesh zone was created and set to the named selection "Piston Head" with "y_motion" as the indicated (imported) velocity profile, dictating the reciprocating motion of the piston in the cylinder. A similar profile was created for the Port with pressure and time as the fields. The text for the velocity and pressure profiles are available in Appendix E. ANSYS Pressure and Velocity ProfilesPressure was alternated between 206 kPa gage and 0 kPa gage (relative pressure was set to 101 kPa). The velocity profile for the piston resembles a saw tooth with constant velocity up then down and the pressure profile resembles a step function with pressure being turned on instantly for a time then turned off.

Actual operation resembles a sine wave. The expected differences in the simulation are a rapid reversal of the flow rather than a gradual that would be seen with a sine wave. 30 seconds of operation were simulated at 60 RPM. Once these settings were input, the simulation has to be initialized prior to the solver being ran. Hybrid initialization was used.

C. RESULTS

The ANSYS results for flow velocity were as expected. The flow came in through the port and filled the chamber, with flow going down the cylinder wall opposite of the port and then recirculating up. This can be seen with the velocity vectors in Figure 32 and Figure 33.

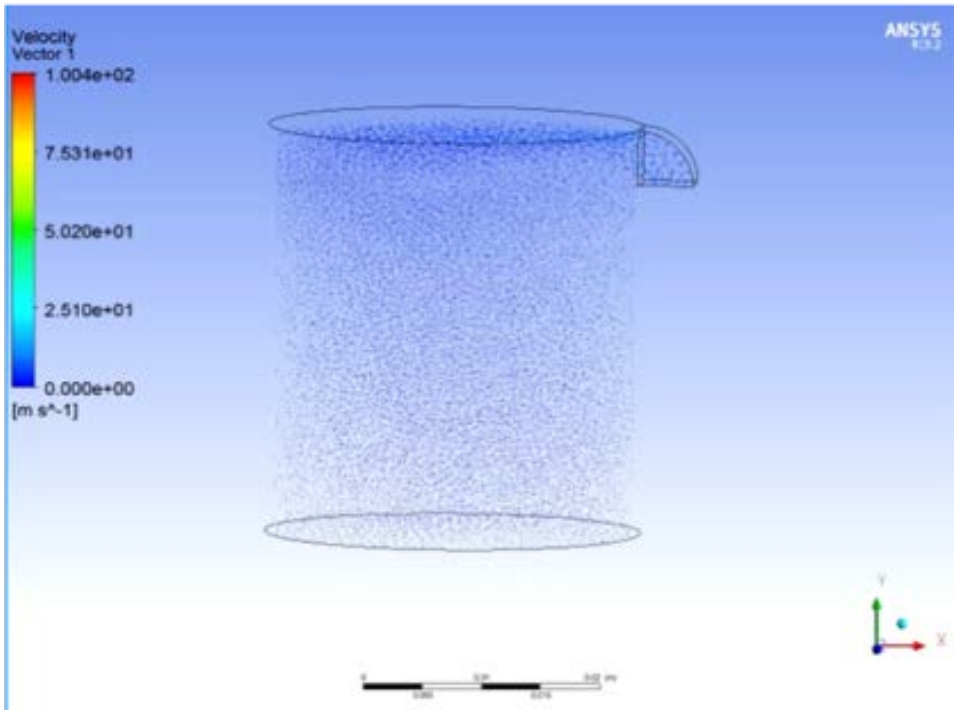

Figure 32. Velocity Vectors for Out Flow

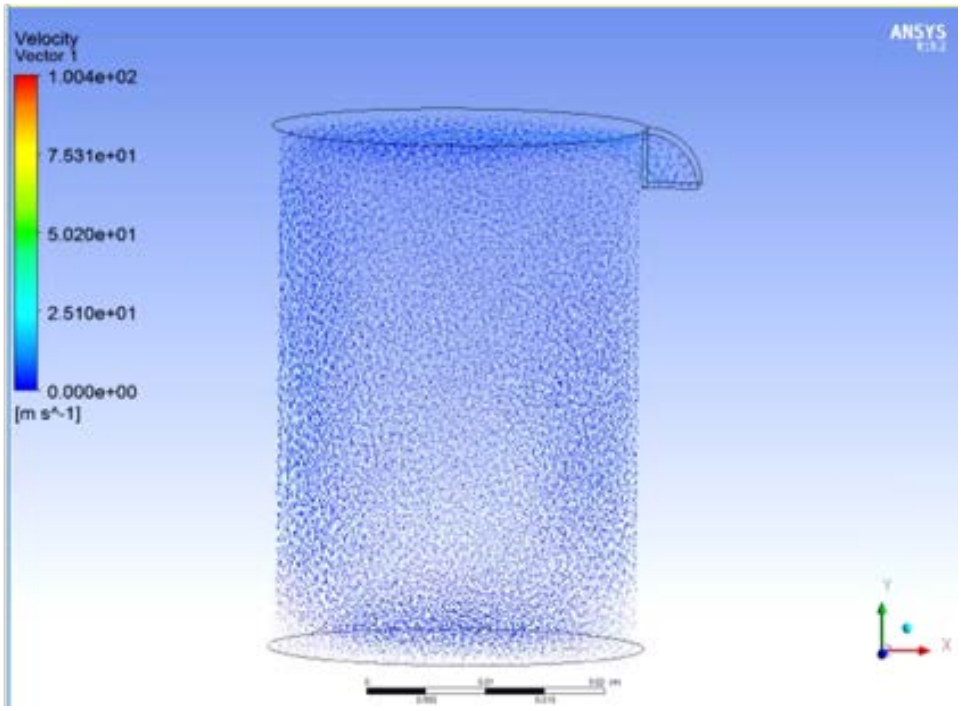

Figure 33. Velocity Vectors for In Flow

Mass flow rate results were not as expected. The simulation was setup to replicated one second of operation at approximately 500 RPM at 206.8 kPa (30 PSI). Based on the operating curves from the manufacturer, this should have produced a mass flow rate of approximately $3x10^{-3}$ kg/s (5 SCFM using the density of air at 20° C). The air consumption curves are shown in Figure 34.

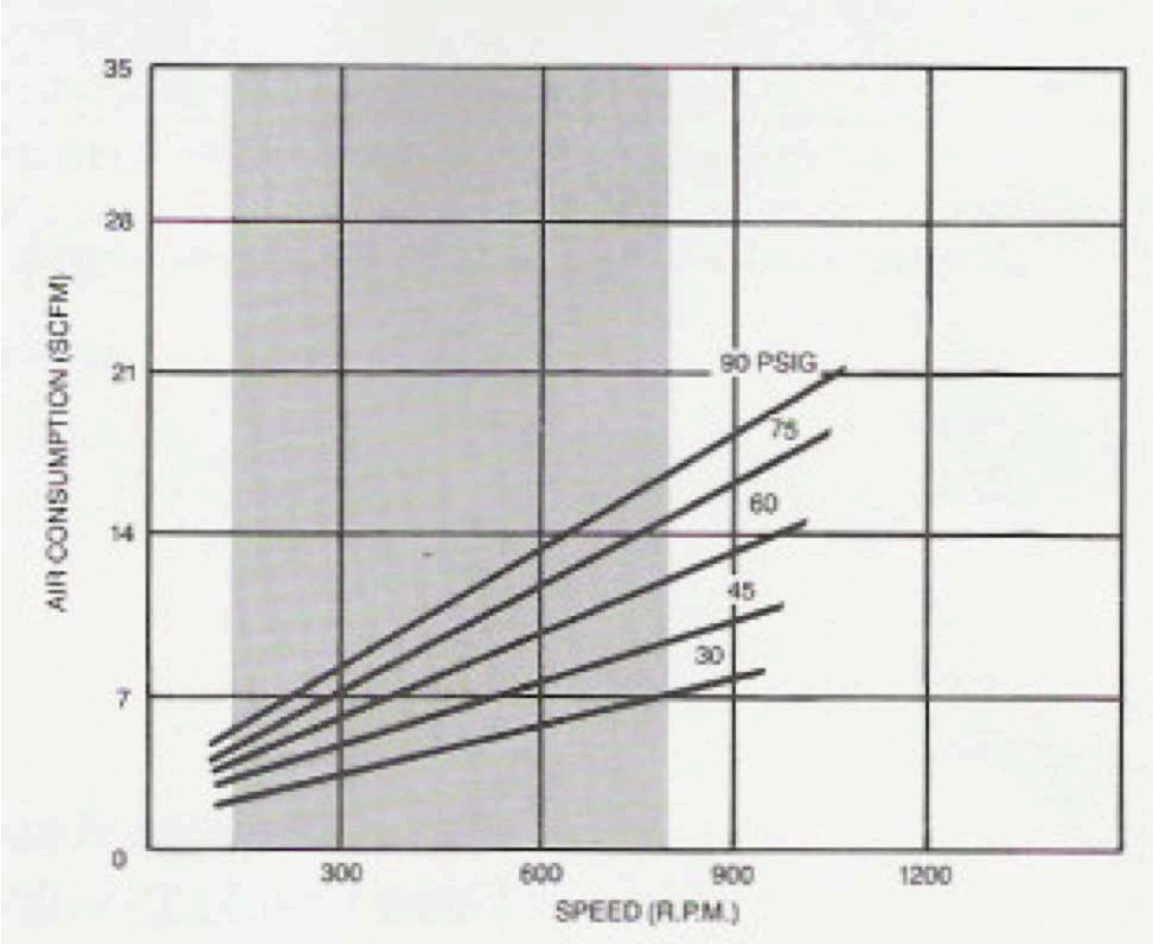

Figure 34. Air Consumption for the UTAM4-030 Radial Air Motor. Source: [5].

Mass flow rate is shown as a plane cross section across the Z-axis of the cylinder on the up and down strokes, with outflow in Figure 35 and inflow in Figure 36. Possibly causes of the results not being as expected are limitations with the solver or the mass flow measurement being placed at the across a large Z axis plane. Rather than measuring mass flow rate within the cylinder, a better location would be at the boundary condition of the Inlet/Outlet Port. The cross sectional area of the port is small and allows for a more accurate representation than the cross section of the middle of the cylinder. Further, as the piston was not moving in response to the pressure changed, the mass flow was not modeled accurately.

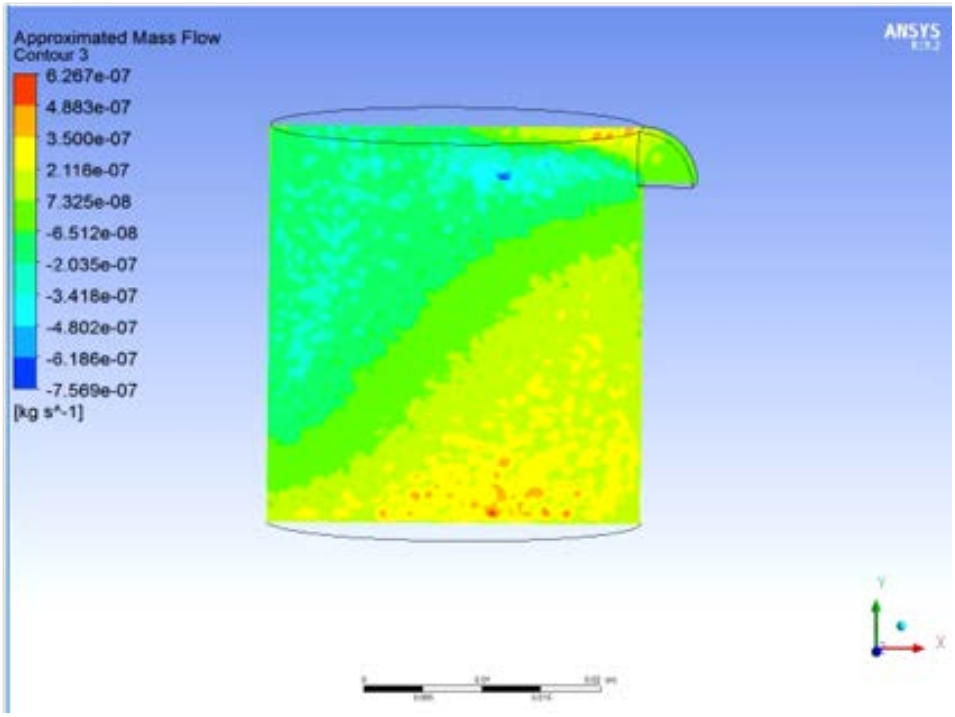

Figure 35. Out Flow Mass Flow Rate

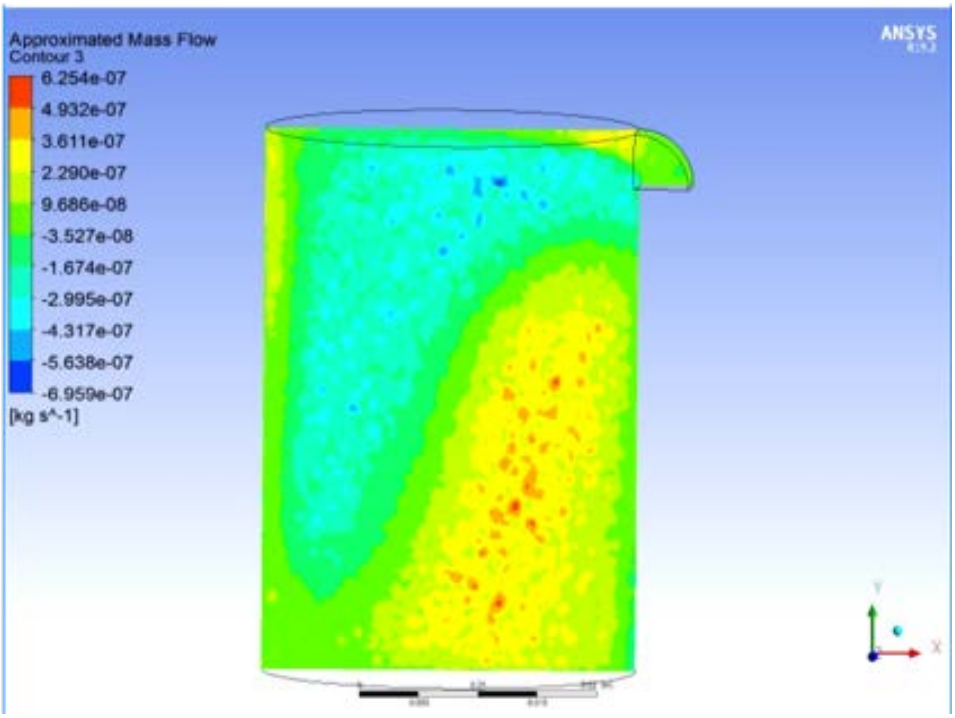

Figure 36. In Flow Mass Flow Rate

VI. CONCLUSION

A. FUTURE WORK

1. Optimization

This system as assembled is the best performing iteration thus far. Optimization of the system to find the ideal speed for the air motor operation to match the maximum output of the generator is the next step. Possible use of a gear box to step up the speed of the shaft speed of the air motor would have the greatest impact, allowing the air motor to operate entire within the prescribed power band. While the air motor began operation at the max power in the available band with the 80 KV motor, by the end of the run it was outside of the recommended maximum operating speed. A gear box would allow for throttling of the input air to control speed, while still operating the generator at speeds sufficient to charge the capacitor. Over time, continued operation outside of the band could have detrimental effects on the motor or the generator. Currently, there are not any PMG Motors with an RPM for Volt rating of less than 80 KV available in the open access market, limiting the possibility of an extraction system with lower KV rated generators

2. Smaller Air Motor

Another option to bring the motor speed lower in the control band would be to use a smaller air motor that has less power. The five cylinder air motor was over powered for this application. The manufacturer offers two different three cylinder options, one with the bore size the same as the five cylinder and one with a slightly smaller bore size, providing different power options. Further exploration of differently sized radial air motors, could result in better performance characteristics. Further, reduction in the air motor size (along with a smaller size generator) would bring this system from the small-scale to the micro-scale, opening up the possibility of man-portable sized systems.

B. RECOMMENDATIONS

1. Control System Integration

A control system was developed to measure capacitor voltage level and to open an air control valve in response to maintain the capacitor voltage at a desired level. This control system while verified to function, has not yet been integrated with the energy extraction system. Full system integration with the control system installed will provide different operating dynamics of the extraction system as it will not be recharging the capacitor from a completely discharged state.

2. Shipboard Applications and Other Uses

All U.S. Navy ships are equipped with vital combat systems suites, integrated networks, and essential communications equipment. These same ships also have compressed air systems on board, from control air at less than 207 kPa (30 PSI) to high pressure systems at over 27.58 MPa (4000 PSI). The radial air motor used in this extraction system is rated to operate at pressures as low as 207 kPa (30 PSI) and up to 620 kPa (90 PSI), allowing for a wide operating range to utilize all available air pressure sources on a ship. Integration of CAES Extraction into current systems would allow for continuity of power to vital and sensitive equipment during prolonged interruptions of the regular power supplies that are damaged if not powered off correctly. Furthermore, many large pieces of equipment require large startup currents when being started. A built in capacitor, recharged from the ship's existing air supply, would minimize this startup current, allowing for the ship's electrical system to be more resilient and battle ready.

Further miniaturization to create man-portable systems would allow for infantry personnel to carry their own power generation systems while in the field with underdeveloped or unreliable grids. A small expander is not dependent upon just compressed air to power the system, allowing the use of any compressed gas available. This would reduce or even eliminate excessive battery requirements and free the user of the limitations associated with the reduced battery performance in cold environments.

APPENDIX A. UTAM4-030 OPERATING CURVES

SPECIFICATIONS

Model No. \ Item		Type	Gear Ratio	*Max. Power				Staring Torque ft-lb	Stall Torque ft-lb	Max. Allowable Shaft Load		Weight		
				Horse Power hp	Torque ft-lb	Speed rpm (Ref)	Air Consumption scfm			Radial Load lb	Thrust Load lb	Direct Drive lb	Flange Mount lb	Foot Mount lb
UTAM4-010	S	Direct Drive	—	0.10	0.47	1100	7	0.51	0.87	22	13	3.2	3.3	4.6
	G005	Geared Drive	1/5	0.09	2.09	220		2.16	3.61	55	33	—	6.6	6.4
	G010		1/10		4.19	110		4.33	7.22	121	55			
	G020		1/20		8.44	55		8.66	15.55	242	99			
UTAM4-015	S	Direct Drive	—	0.17	1.01	900	9.2	1.44	2.16	31	22	5.5	5.7	7.5
	G005	Geared Drive	1/5	0.15	4.33	180		6.49	9.38	88	55	—	11.2	11.0
	G010		1/10		8.66	90		12.99	19.48	176	77			
	G020		1/20		17.32	45		25.98	38.97	308	154			
UTAM4-030	S	Direct Drive	—	0.31	2.16	750	14.1	3.46	4.33	44	31	10.1	10.6	14.1
	G005	Geared Drive	1/5	0.27	9.38	150		15.15	19.48	110	66	—	19.6	19.4
	G010		1/10		19.48	75		30.31	38.97	220	99			
	G020		1/20		38.97	38		60.61	77.93	396	187			
Media		Filtered (Under 40μm) and lubricated air												
*Max. Operating Pressure		90 psig (7kgf/cm^2)												
Ambient and media temperature		32 ~ 158°F (0 ~ 70°C) at no freezing condition.												
**Lubrication for line lubricators		Should be necessary/Recommended oil; misting-type oils rated 150-200 SSU at 100°F (38°C)/ISO VG 32												
**Recommended gear oil		Same as Shell Oil Co. Alvania #EP RIO 71039 Grade "00" or Sun Petroleum Products Prestige 740 AEP Grade "00"												

* These Motors must be operated with sufficient load to prevent speed from exceeding maximum allowable speed shown on performance curve. Do not operate motors at more than 80% of or near Max. power speed.

** The oil used must be compatible with materials of construction. Contact your lubricant supplier and the builder of equipment to be lubricated to obtain lubricant recommendations.
The proper grades of grease and oil are essential to the economical operation of any air motor.

UTAM4-030S

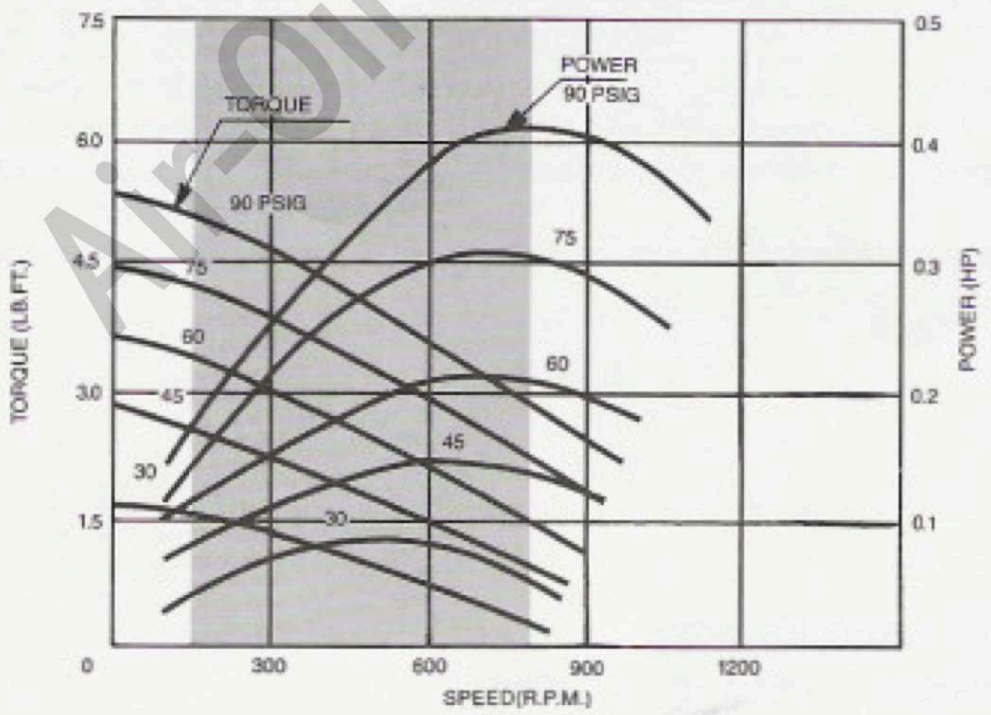

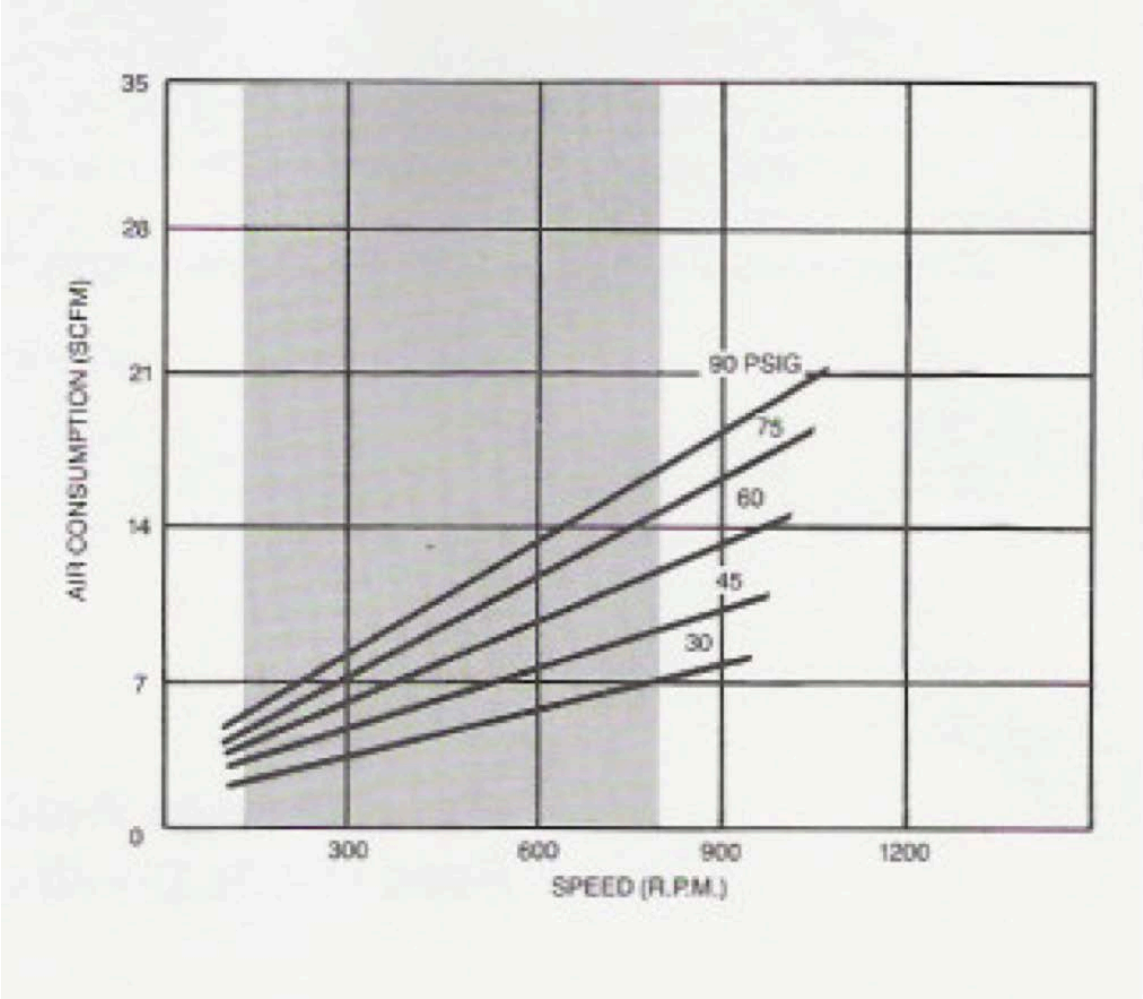
35
28
21
14
7
0
AIR CONSUMPTION (SCFM)
90 PSIG
75
60
45
30
300
600
900
1200
SPEED (R.P.M.)

Source: [5].

APPENDIX B. 3D-PRINTED COUPLING DEVICE

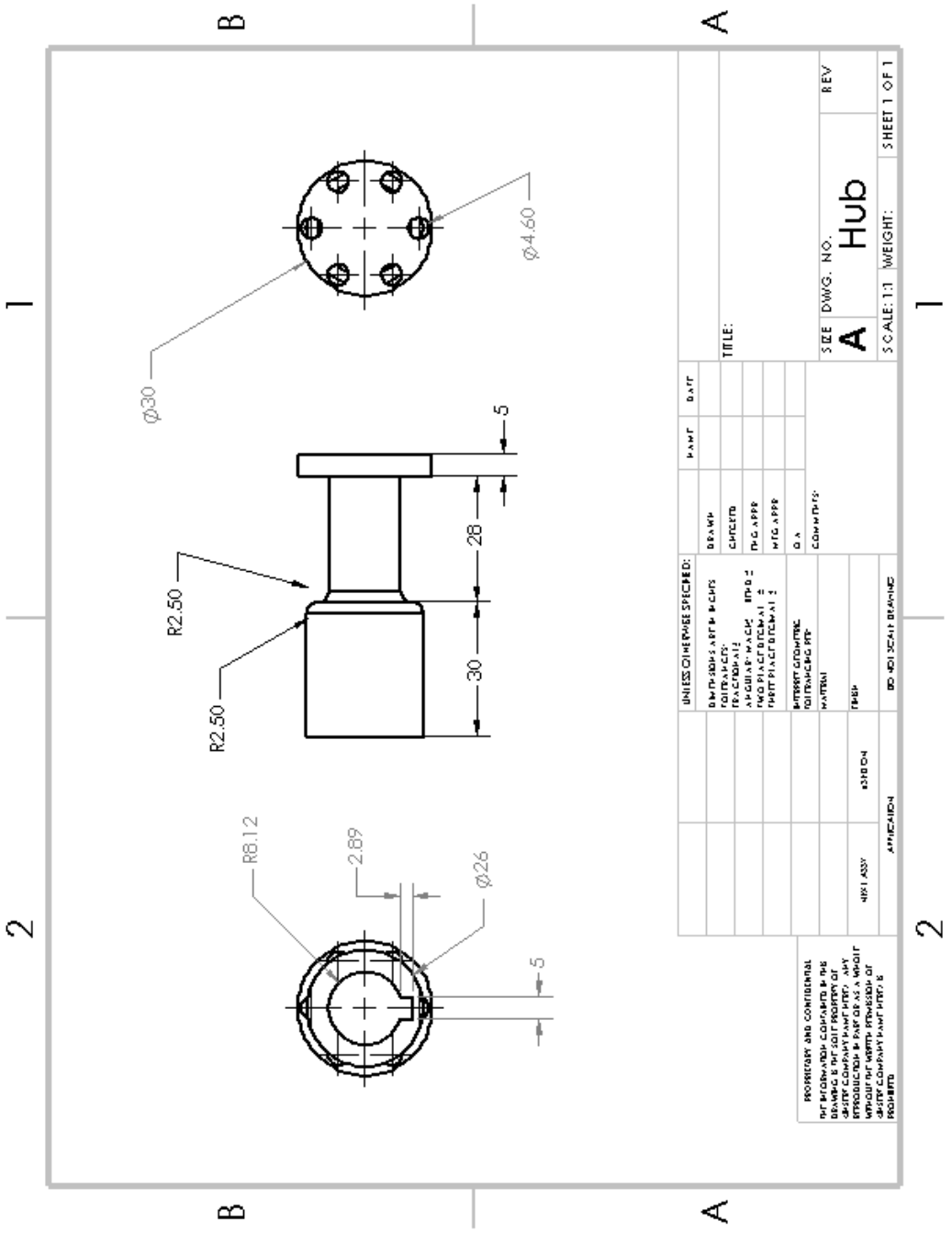

THIS PAGE INTENTIONALLY LEFT BLANK

APPENDIX C. MATLAB CODE USED TO PLOT DATA FROM RUN FIGURES

Contents

Pulling Data from saved MATLAB Figures

```
kids = get(gca,'children');
for iii = 1:length(kids)
    xxx = get(kids(iii),'xdata');
    yyy = get(kids(iii),'ydata');
    dn = get(kids(iii),'displayname') ;
    % in the event that you need the name for some reason
    fname = [datestr(now,'yyyymmdd_HHMMSSFFF') '_datafile.txt']
    [fid,status] = fopen(fname,'w');

end
```

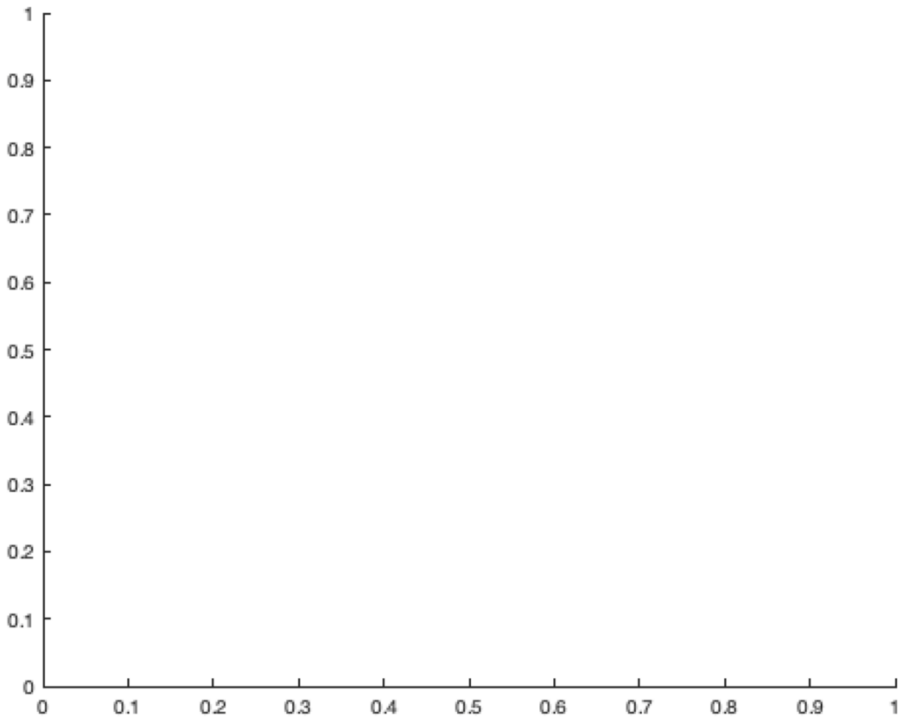

RPM

figure(1)

```
yyx=(yyy+1000)./2;
yyt=transpose(yyx);
% plot(xxx,yyy,xxx,yyx); %commented to remove plot from Publish
xlabel('Time (s)')
ylabel('RPM')
x=linspace(0,2000,21);
xticks(x);
xtickangle(90);
ylim([-300 1500])
xlim([0 1500])
title({'80 KV (with flow restriction)','RPM vs Time'})
legend('Orginal Data RPM','Corrected RPM','Location','southeast')
grid on
```

```
Warning: Ignoring extra legend entries.
```

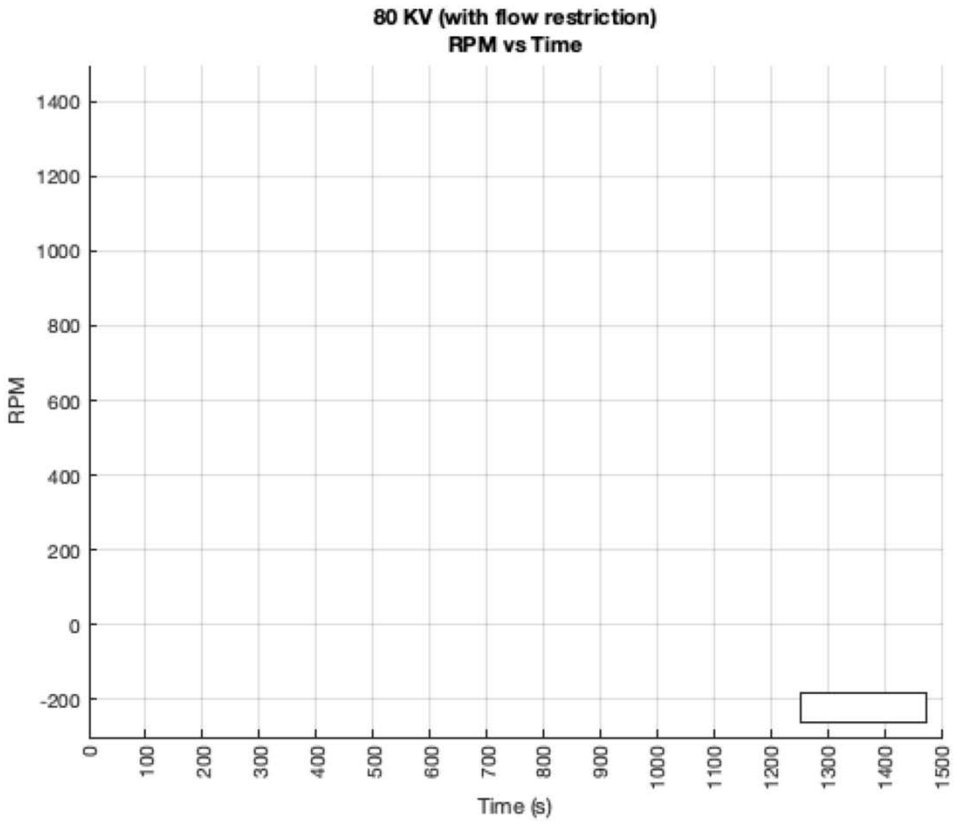

Capacitor Voltage

figure(1) plot(xxx,yyy) %commented to remove plot from Publish

```
xlabel('Time (s)')
ylabel('Capacitor Voltage (volts)')
x=linspace(0,2000,21);
xticks(x);
xtickangle(90);
ylim([0 60])
xlim([0 800])
title({'80 KV (without flow restriction)','Voltage vs Time'})
legend('Capacitor Voltage','Location','southeast')
grid on
```

```
Warning: Ignoring extra legend entries.
```

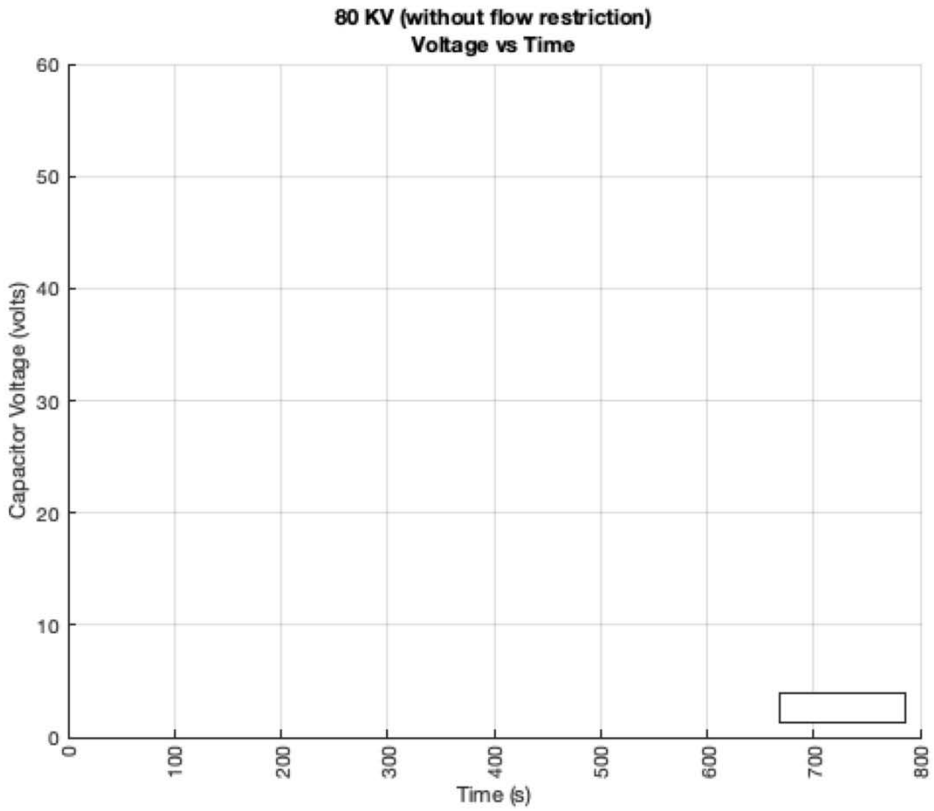

CURRENT CALCS

```
windowSize = 10;
b = (1/windowSize)*ones(1,windowSize);
a = 1;
I = 130.*(diff(yyy)./diff(xxx));
If = smoothdata(filter(b,a,I));
%figure(2)
%plot(xxx(2:end),I) %commented to remove plot from Publish
hold on
%plot(xxx(2:end),If,'Linewidth',1.5) %commented to remove plot from Publish
xlabel('Time (s)')
ylabel('Current (amps)')
x=linspace(0,2000,21);
xticks(x);
xtickangle(90);
```

```
ylim([0 25])
xlim([0 800])
title({'80 KV (without flow restriction)','Current vs Time'})
legend('Current','Current (filtered)','Location','best')
grid on
```

```
Warning: Ignoring extra legend entries.
```

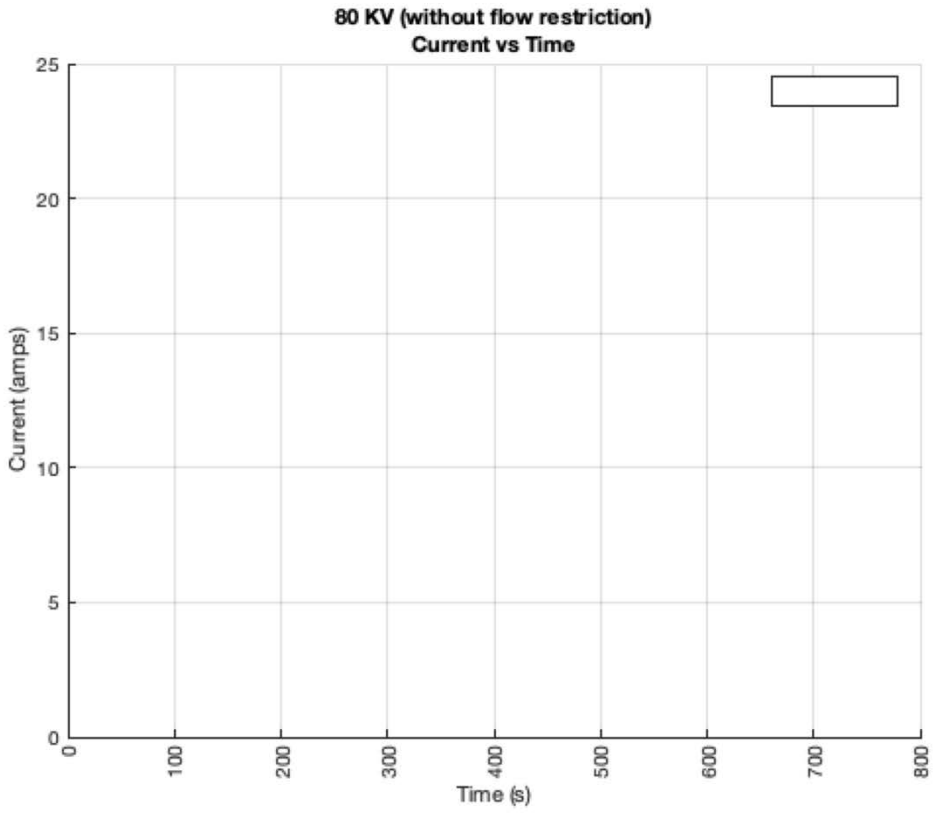

POWER CALCS

```
%figure(1)
%plot(xxx,yyy) %commented to remove plot from Publish
hold on
windowSize = 20;
b = (1/windowSize)*ones(1,windowSize);
a = 1;
Pf = smoothdata(filter(b,a,yyy));
```

```
%plot(xxx,Pf,'Linewidth',1.5) %commented to remove plot from Publish
xlabel('Time (s)')
ylabel('Power (watts)')
x=linspace(0,2000,21);
xticks(x);
xtickangle(90);
ylim([0 500])
xlim([0 800])
title({'80 KV (without flow restriction)','Power vs Time'})
legend('Power','Power (filtered)','Location','southeast')
grid on
```

```
Warning: Ignoring extra legend entries.
```

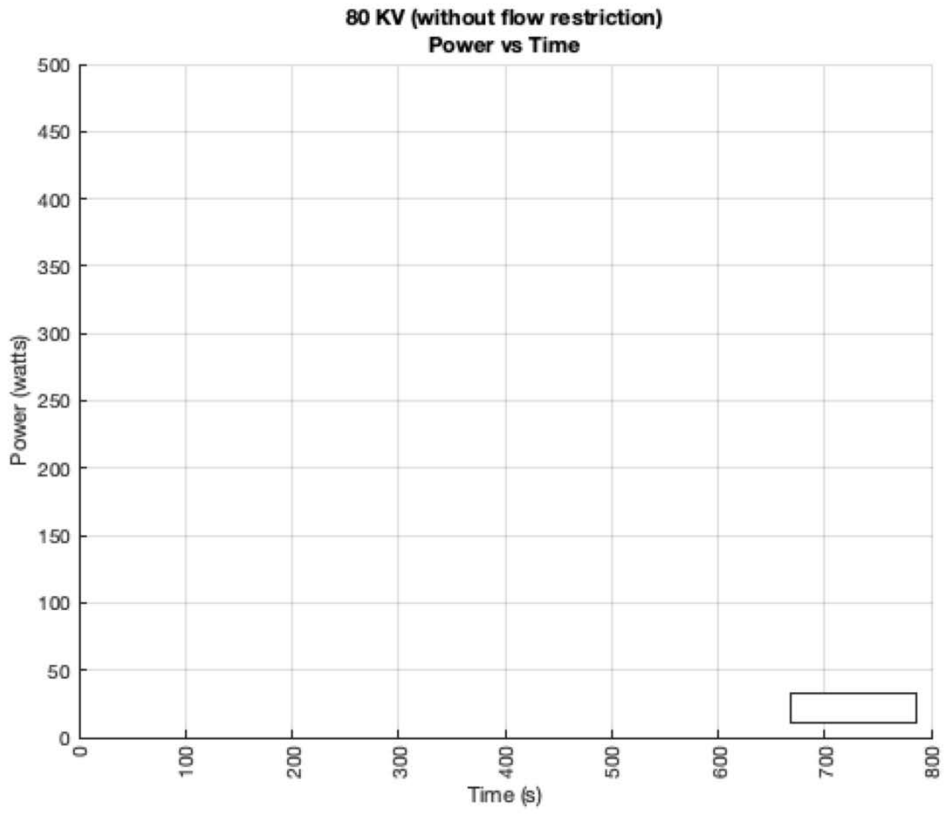

Published with MATLAB® R2018a

APPENDIX D. MATLAB CODE USED TO RECORD DATA FROM EACH RUN

Contents


```
clear all
close all
clc

devices = daq.getDevices;
ni_set = daq.createSession('ni');

ni_set.Rate = 4;

 addAnalogInputChannel(ni_set,'Dev1',0:3,'Voltage');
 for iii=1:numel(ni_set.Channels)
    ni_set.Channels(iii).TerminalConfig = 'Differential';
 end

JM_pbricksetup

vp = plot(NaN,NaN,'-');
pp = plot(NaN,NaN,'-');
rp = plot(NaN,NaN,'-');
ip = plot(NaN,NaN,'-');
pwrp = plot(NaN,NaN,'-');
Farad = 130; % Capacitor Farad Rating
```

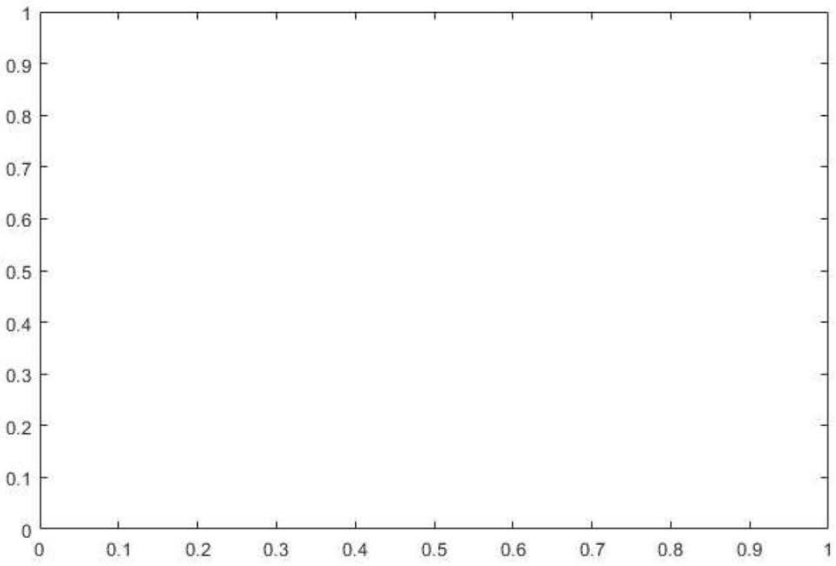

Voltage Plot

```
subplot(5,1,1)
vp = plot(NaN,NaN,'-');
title('Capacitor Voltage')
xlabel('Time (s)')
ylabel('Voltage (DC)')
```

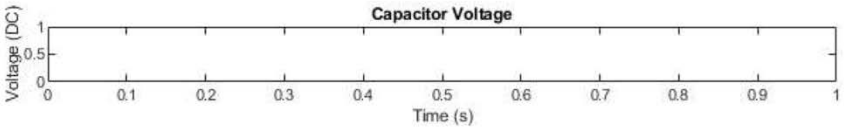

Current Plot

```
subplot(5,1,2)
ip = plot(NaN,NaN,'-');
title('Current')
xlabel('Time (s)')
ylabel('Current (Amps)')
```

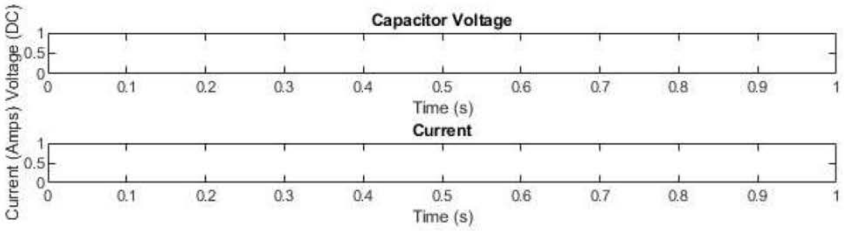

Pressure Plot

```
subplot(5,1,3)
pp = plot(NaN,NaN,'-');
title('Air Pressure (PSI)')
xlabel('Time (s)')
ylabel('Pressure')
```

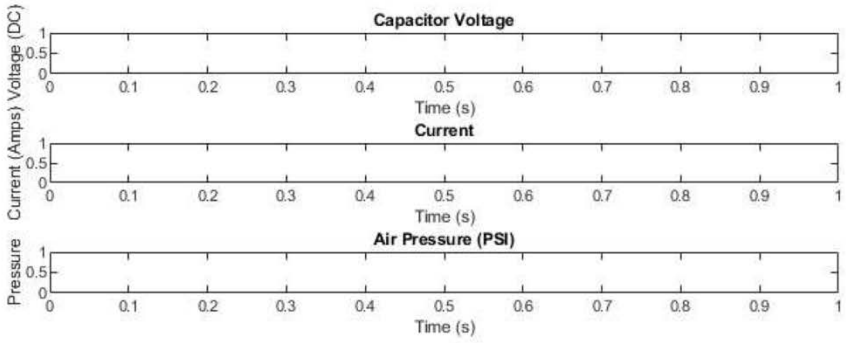

RPM Plot

```
subplot(5,1,4)
rp = plot(NaN,NaN,'-');
title('RPM')
xlabel('Time (s)')
ylabel('RPM')
```

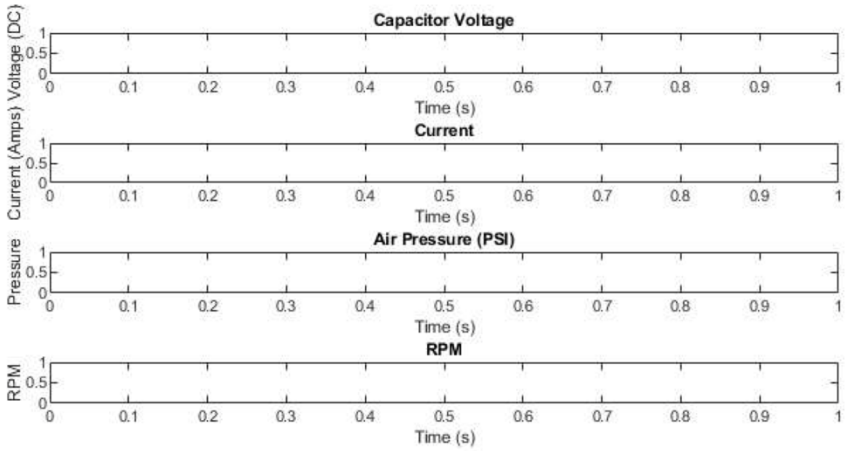

Power Plot

```
subplot(5,1,5)
pwrp = plot(NaN,NaN,'-');
title('Power')
xlabel('Time (s)')
ylabel('Power (Watts)')

endtime = 180;
hui= uicontrol('Style','edit','String',num2str(endtime));

iii=1;
while iii<endtime
ni_set.DurationInSeconds = 1;
event.data = startForeground(ni_set);
fprintf(pbrick1, 'SCAN'); % this is just a reading function
output = ws_readPressureBrickData(pbrick1,pbrickvars);
Capvolts=(mean(event.data(:,1))*7.5)-.37;
rpm = (max((event.data(:,2))*1000));
%rpm = filter(b,a,rpmx);
Charge(iii) = Farad*Capvolts;
if iii>1
    I = (Charge(iii)-Charge(iii-1))/1; %ni_set.DurationInSeconds;
    set(ip,'xdata',[get(ip,'xdata') iii],'ydata',[get(ip,'ydata') I]);
    Power=((Capvolts*I));
    set(pwrp,'xdata',[get(pwrp,'xdata') iii],'ydata',[get(pwrp,'ydata') Power]);
end


set(vp,'xdata',[get(vp,'xdata') iii],'ydata',[get(vp,'ydata') Capvolts]);
set(pp,'xdata',[get(pp,'xdata') iii],'ydata',[get(pp,'ydata') output.Pressures(1)/6890]);
```

```
set(rp,'xdata',[get(rp,'xdata') iii],'ydata',[get(rp,'ydata') rpm]);

iii=iii+1;
endtime = str2double(get(hui,'String'));
end



ni_set.stop
JM_pbrickclose

fname = '80KvRun2';
csvwrite(fname,[get(vp,'xdata')' get(vp,'ydata')' get(pp,'ydata')' get(rp,'ydata')' [0;get(ip,'ydata
')'] [0;get(pwrp,'ydata')']])
```

```
pbrickvars =
  struct with fields:

       PERIOD: '3906'
          AVG: '16'
          FPS: '1'
    XSCANTRIG: '0'
       FORMAT: '0'
         TIME: '2'
           EU: '1'
           ZC: '1'
          BIN: '0'
          SIM: '0'
        QPKTS: '0'
     UNITSCAN: 'PA'
      CVTUNIT: '6894.759766'
         PAGE: '0'
```

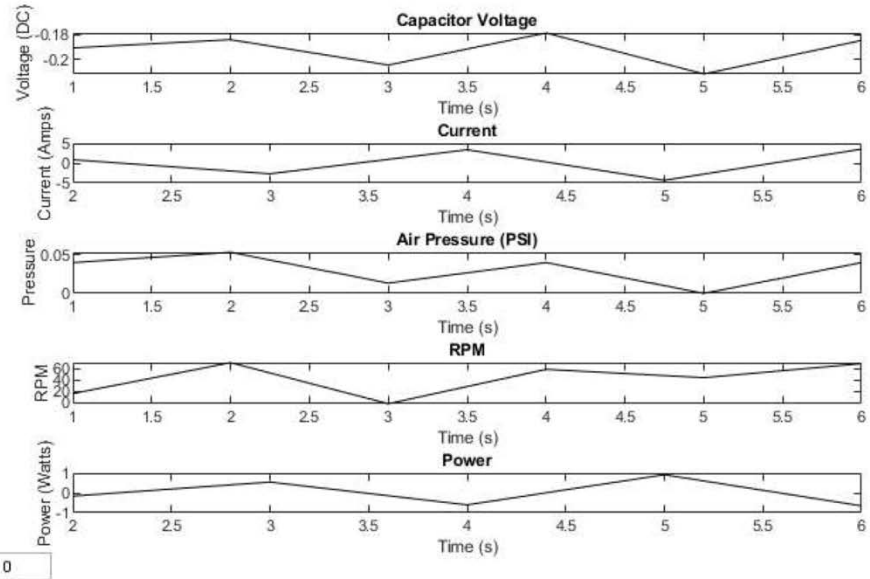

0

Published with MATLAB® R2018b

```
TotalAcquisitionTime = 1;
% Dont Set data rate higher than 24 for pressure bricks.
DataRate = 1; % Samples per second, equivalent to Frames per Second...
if DataRate> 32, DataRate = 32;fprintf('Main\t::\tYour Data Rate was set too high... setting
to a tested high value (32 Hz).\n');end
setavg = 240; % number of samples to acquire before producing averaged output 1 -> 240
% setAvgMax = 10^(-1*log10(DataRate)+3);if setavg > setAvgMax, setavg = floor(setAvgMax);fpri
ntf('Main\t::\tThe Number of averages per Frame was set too high for the data acquisition rat
e.\nMain\t::\tSetting to the max for the rate: %f\n',setavg);end
setavg = 16; % set to minimum for best transient results.
settime = 2; % set to output format so that a Time after scan start is given.
setfps = TotalAcquisitionTime*DataRate; % The number of frames to acquire...
setperiod = (1./(DataRate * 16 * setavg))*10^6; % the acquisition period for each channel in
mirco-seconds
setUnits = 'PA'; % Use SI/Pascals
setEU = 1; % Use Engineering Units
setZC = 1; % ensure the use of Zero Correction.
setBIN = 0; % make data acquisition in ASCII format.
setQPKTS = 0; % what to do with frame buffer if not read in time-- trash it.


% hmifig = figure(1);
% ud.DataRate = DataRate;
% ud.tmp = 1010;
% hui.dataRate_text = uicontrol('Style','text','Parent',hmifig,...
%     'Units','normalized','Position',[0 0 .1 .05],...
%     'FontWeight','bold','FontUnits','normalized',...
%     'String',['f_s = ' num2str(DataRate) ' Hz '],'Tag','dataRate_text','UserData',ud);
% clear ud


pbrickvars.UNITSCAN = num2str(setUnits); % Why a string? I'm lazy.
pbrickvars.EU = num2str(setEU);
pbrickvars.BIN = num2str(setBIN);
pbrickvars.FPS = num2str(setfps);
pbrickvars.QPKTS = num2str(setQPKTS);
pbrickvars.TIME = num2str(settime);
pbrickvars.AVG = num2str(setavg);
pbrickvars.PERIOD = num2str(setperiod);


% Connect DSA pressure bricks and set parameters
    pbrick1 = instrfind('Type', 'tcpip', 'RemoteHost', '191.30.80.234', 'RemotePort', 23, 'Ta
g', 'pbrick1');
   % Create the tcpip object if it does not exist
    % otherwise use the object that was found.
    if isempty(pbrick1),pbrick1 = tcpip('191.30.80.234', 23, 'Tag', 'pbrick1');
    else fclose(pbrick1);pbrick1 = pbrick1(1);end

    %Connect to instrument objects.
    fopen(pbrick1);

%     pbrickvars = ws_setPressureBrickParameters(pbrick1,pbrickvars);
%     pbrickvars = ws_getPressureBrickParameters(pbrick1)
    output = ws_setPressureBrickParameters(pbrick1,pbrickvars)
```

```
fprintf(pbrick1, 'SCAN'); % this is just a reading function
output = ws_readPressureBrickData(pbrick1,pbrickvars)


    pbrickvars = ws_getPressureBrickParameters(pbrick1)
    fclose(pbrick1)

    output.Pressures(1)
```

```
output =
  struct with fields:

       PERIOD: '3906'
          AVG: '16'
          FPS: '1'
    XSCANTRIG: '0'
       FORMAT: '0'
         TIME: '2'
           EU: '1'
           ZC: '1'
          BIN: '0'
          SIM: '0'
        QPKTS: '0'
     UNITSCAN: 'PA'
      CVTUNIT: '6894.759766'
         PAGE: '0'
output =
  struct with fields:

        framenum: 0
            time: 0.9370
        Channels: [16×1 double]
       Pressures: [16×1 double]
    Temperatures: [16×1 double]
pbrickvars =
  struct with fields:

       PERIOD: '3906'
          AVG: '16'
          FPS: '1'
    XSCANTRIG: '0'
       FORMAT: '0'
         TIME: '2'
           EU: '1'
           ZC: '1'
          BIN: '0'
          SIM: '0'
        QPKTS: '0'
     UNITSCAN: 'PA'
      CVTUNIT: '6894.759766'
         PAGE: '0'
ans =
  366.0625
```

```
TotalAcquisitionTime = 1;
% Dont Set data rate higher than 24 for pressure bricks.
DataRate = 1; % Samples per second, equivalent to Frames per Second...
if DataRate> 32, DataRate = 32;fprintf('Main\t::\tYour Data Rate was set too high... setting
to a tested high value (32 Hz).\n');end
setavg = 240; % number of samples to acquire before producing averaged output 1 -> 240
% setAvgMax = 10^(-1*log10(DataRate)+3);if setavg > setAvgMax, setavg = floor(setAvgMax);fpri
ntf('Main\t::\tThe Number of averages per Frame was set too high for the data acquisition rat
e.\nMain\t::\tSetting to the max for the rate: %f\n',setavg);end
setavg = 16; % set to minimum for best transient results.
settime = 2; % set to output format so that a Time after scan start is given.
setfps = TotalAcquisitionTime*DataRate; % The number of frames to acquire...
setperiod = (1./(DataRate * 16 * setavg))*10^6; % the acquisition period for each channel in
mirco-seconds
setUnits = 'PA'; % Use SI/Pascals
setEU = 1; % Use Engineering Units
setZC = 1; % ensure the use of Zero Correction.
setBIN = 0; % make data acquisition in ASCII format.
setQPKTS = 0; % what to do with frame buffer if not read in time-- trash it.


% hmifig = figure(1);
% ud.DataRate = DataRate;
% ud.tmp = 1010;
% hui.dataRate_text = uicontrol('Style','text','Parent',hmifig,...
%     'Units','normalized','Position',[0 0 .1 .05],...
%     'FontWeight','bold','FontUnits','normalized',...
%     'String',['f_s = ' num2str(DataRate) ' Hz '],'Tag','dataRate_text','UserData',ud);
% clear ud


pbrickvars.UNITSCAN = num2str(setUnits); % Why a string? I'm lazy.
pbrickvars.EU = num2str(setEU);
pbrickvars.BIN = num2str(setBIN);
pbrickvars.FPS = num2str(setfps);
pbrickvars.QPKTS = num2str(setQPKTS);
pbrickvars.TIME = num2str(settime);
pbrickvars.AVG = num2str(setavg);
pbrickvars.PERIOD = num2str(setperiod);


% Connect DSA pressure bricks and set parameters
    pbrick1 = instrfind('Type', 'tcpip', 'RemoteHost', '191.30.80.234', 'RemotePort', 23, 'Ta
g', 'pbrick1');
   % Create the tcpip object if it does not exist
    % otherwise use the object that was found.
    if isempty(pbrick1),pbrick1 = tcpip('191.30.80.234', 23, 'Tag', 'pbrick1');
    else fclose(pbrick1);pbrick1 = pbrick1(1);end

    %Connect to instrument objects.
    fopen(pbrick1);

%     pbrickvars = ws_setPressureBrickParameters(pbrick1,pbrickvars);
%     pbrickvars = ws_getPressureBrickParameters(pbrick1)
    output = ws_setPressureBrickParameters(pbrick1,pbrickvars);
```

```
    pbrickvars = ws_getPressureBrickParameters(pbrick1)
    fclose(pbrick1)

    output.Pressures(1);
```

```
pbrickvars =
  struct with fields:

       PERIOD: '3906'
          AVG: '16'
          FPS: '1'
    XSCANTRIG: '0'
       FORMAT: '0'
         TIME: '2'
           EU: '1'
           ZC: '1'
          BIN: '0'
          SIM: '0'
        QPKTS: '0'
     UNITSCAN: 'PA'
      CVTUNIT: '6894.759766'
         PAGE: '0'
```

APPENDIX E. ANSYS PRESSURE AND VELOCITY PROFILES

Pressure Profile

(Port Press 7 point)
(time 0 10 20 30 40 50 60)
(p_y 0 300000 0 300000 0 300000 0))

Velocity Profile

((y_motion 31 point)
(time 0 1 2 3 4 5 6 7 8 9 10 11 12 13 14 15 16 17 18 19 20 21 22 23 24 25 26 27 28 29 30)
(v_y 0.0282 -0.0282 0.0282 -0.0282 0.0282 -0.0282 0.0282 -0.0282 0.0282 -0.0282 0.0282 -0.0282 0.0282 -0.0282 0.0282 -0.0282 0.0282 -0.0282 0.0282 -0.0282 0.0282 -0.0282 0.0282 -0.0282 0.0282 -0.0282 0.0282 -0.0282 0.0282))

THIS PAGE INTENTIONALLY LEFT BLANK

LIST OF REFERENCES

[1] Ramadan, O., Omer, S., Jradi, M, Sabir, H., and Riffat, S., 2016, "Analysis of compressed air energy storage for large-scale wind energy in Suez, Egypt," *International Journal of Low-Carbon Technologies*, 11, pp. 476–488.

[2] He, W. and Wang, J, 2018,"Optimal selection of air expansion machine in Compressed Air Energy Storage: A review," *Renewable and Sustainable Energy Reviews*, 87, pp. 77–95.

[3] McLaughlin, C. S., 2016, "Small-scale air-driven generator," Master's Thesis, Naval Postgraduate School, Monterey, CA.

[4] Pelletier, N. S., 2018, "Small-scale power extraction system for Compressed Air Energy Storage," Master's Thesis Naval Postgraduate School, Monterey, CA.

[5] "AirOil.com Assets Air Motor Specs," accessed January 10, 2020, https://www.airoil.com/uploads/assets/downloads/airpromotor.pdf.

[6] "Emerson Industrial Transformers," last modified December 2018, https://www.emerson.com/documents/automation/catalog-solahd-sbe-series-transformers-en-us-163796.pdf.

[7] "Digi-Key Electronics MSD100-12 Datasheet," last modified December 2009, accessed January 27, 2020 https://www.digikey.com/product-detail/en/microsemi-corporation/MSD100-12/MSD100-12-ND/2260207.

[8] "Maxwell.com 56V Modules Datasheet," accessed January 15, 2020 https://www.maxwell.com/images/documents/56vmodule_ds_1017119-3.pdf.

[9] "National Instruments USB-6003 Overview," accessed January 15, 2020, https://www.ni.com/documentation/en/multifunction-io-device/latest/usb-6003/overview/.

[10] K. Tweed, "Toronto Hydro pilots world's first offshore compressed-air energy storage project," Green Tech Media, November 25, 2015, https://www.greentechmedia.com/articles/read/toronto-hydro-pilots-worlds-firstoffshore-compressed-air-energy-storage#gs.oYV72ng.

[11] "AEO Machine Products 3000L 13Bar Industrial Air Tank," accessed December 27, 2019, http://www.aeomachine.com/html/en/products/airtankreceiver/105.html.

[12] Kenneth E. Nichols P.E. "How to select turbomachinery for your application," Barber-Nichols Inc., accessed March 2, 2020, https://www.barber-nichols.com/sites/default/files/wysiwyg/images/how_to_select_turbomachinery_for_your_application.pdf.

THIS PAGE INTENTIONALLY LEFT BLANK

INITIAL DISTRIBUTION LIST

1. Defense Technical Information Center
   Ft. Belvoir, Virginia

2. Dudley Knox Library
   Naval Postgraduate School
   Monterey, California